Statistical Features of A Time-Averaged Global State Estimate: Strong Regional Variations and Implications for Sea Level and Heat Content Change

Carl Wunsch[a]

[a] *Department of Earth and Planetary Sciences, Harvard Un. and Department of Earth, Atmospheric and Planetary Sciences, MIT*

Corresponding author: Carl Wunsch, carl.wunsch@gmail.com

ABSTRACT: A three-dimensional global state estimate derived from Estimating the Circulation and Climate of the Ocean (ECCO) using diverse error-weighted global data permits computation of a multi-decadal time-average ocean circulation and its variability obeying the numerical requirements of the MITgcm and associated property conservation conditions. The result exhibits a variety of underlying temporal structures in different regions: statistically stationary; non-stationary; long memory; short memory; rednoise; bluenoise; etc. That variety renders difficult the interpretation and understanding of quantities such as global averages and trends.The result undermines the hope of simple global-scale description of air-sea interactions of all kinds and leads to the necessity of specific attention to separate regions—but in a fully global context. Specific variables discussed are sea level, and heat content both for the full water column and in the abyss alone with an emphasis on the strong spatial variability of the underlying statistical structures—a result with important consequences for observational sampling strategies. Absent a complete theory for the statistics of very large multivariable time-series, a bootstrap is used to produce estimates of global trends in sealevel and heat content.

SIGNIFICANCE STATEMENT: The recent availability of multi-decadal time-averages of the computed ocean circulation leads to a system with a diverse set of statistical elements which persist for decades and presumably for arbitrarily long time scales. These elements in the underlying time variability, which include stationary and non-stationary, long-memory and short-memory, bluenoise etc., become part of the descriptive oceanography of the general circulation. A strong regionality in air-sea coupling in the climate system is implied, leading to questions about both the use of global means and over-simplified claims of localized global control (e.g., of the North Atlantic meridional overturning circulation). Implications for determination of means and trends are explored.

1. Introduction

That the global ocean circulation contains numerous dynamically distinct regions is an inescapable inference from modern observation systems and models. One example from many is shown in Xu and Fu (2012) using altimeter observations and a dynamical one is Sonnewald et al. (2019). From the greatly intensified near-global ocean observations that became available starting circa 1992, it is now possible to compute estimates of the time-average ocean circulation that span decades. An example of such an estimate, based upon the inverse method of non-linear weighted least-squares fit of the MITgcm (general circulation model) to the great bulk of the available data, is the Estimating the Circulation and Climate of the Ocean (ECCO) result. Lagrange multipliers are used to enforce the model equations. The time-average state estimate was described by Fukumori et al. (2019), and Wunsch (2024, 2025) for ECCO(v4r4), that is version 4, release 4 and spanning T_D =26 years. (T_D has been extended since then, but there is an old rule of thumb in time series analysis that analyses are worth re-doing when the duration has doubled.)

Interpretation of that time-mean raises a number of questions—ones that would apply also to estimates made directly from data without the intervening use of a general circulation model (GCM). Any real, finite-duration ocean time-average exists in a system changing on time-scales far longer than T_D. Fig. 1 provides one approximate depiction of many of those time-scales. Several types exist including time-scales intrinsic to the ocean fluid system (e.g., the high latitude multi-decadal adjustment time of the baroclinic structure of the thermocline—see Anderson et al., 1979) and those induced by long-time-scales in the forcing (e.g., the atmospheric cold period of the

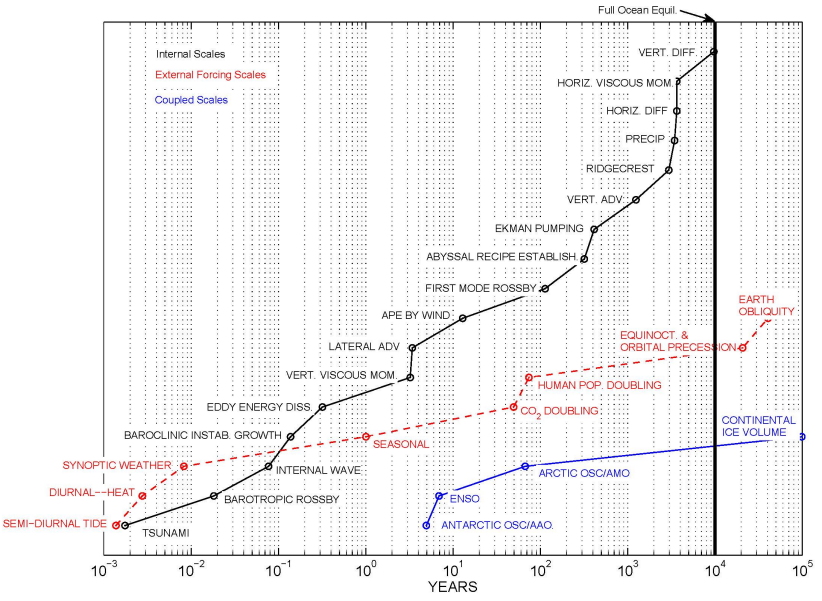

FIG. 1. Approximate time-scales of the changing ocean circulation including those associated with forcing and some of those associated with coupled atmospheric changes. (From Wunsch, 2015.) The vertical axis is used simply to separate the labels and has no dimensions. Some time-scales have characteristic space scales; others have a broad spectrum; but all are global in scope. Abbreviations used include ENSO for El Niño Southern Oscillation; AMO is Atlantic Multidecadal Oscillation; APE is available potential energy; MOM is momentum; DIFF is diffusion; ADV is advection. Many time-scales refer to the replacement time of the global fluid volume by changes in the listed variable. Others arethe sometimes radically shorter trans-oceanic travel times for barotropic and coastal shelf waves. See the reference for a more complete description and interpretation.

Little Ice Age; see Gebbie and Huybers, 2019). A third time-scale arises from the comparatively long-interval between major disturbances such as ENSO—precluding accurate calculation of their long-term average properties.

Particular attention is called to the discussion by Anderson and Gill (1975), Anderson et al (1979) for the understanding of the linearized ocean basin spin-up problem. What emerges are distinct time-scales with a large spatial variation in the basin, with a particular dependence, on east-west position. Topography, such as the North Atlantic Mid-Ocean Ridge, exaggerates those differences.

Questions include, among others: (1) What is the meaning of a finite duration temporal average in a system that contains time-scales far-longer than T_D? (2) Is a particular time-average equivalent

to a real fluid steady-state? (3) Were it possible to calculate an infinite duration time-average under the assumption that the ocean now, or sometime in the past or future, is in an equilibrium state, what spatial elements can be expected to survive the averaging process? That is, what controls the apparent zero-frequency ocean circulation spatial structure? (4) In a statistically inhomogeneous system, what are the accuracy and interpretation of global averages? The purpose here is descriptive and preliminary: to understand the temporal structure of the ocean circulation and begin exploring the extent to which time-means and time-trends can be computed with known accuracy over the almost 30 years of the state estimate.

Of particular societal interest are the means and trends of sea level, heat, and carbon content among others. Wunsch and Heimbach (2016) discussed the generic problems of determining means and trends, and included some results from an earlier state estimate. Wunsch (2018, hereafter W18) discussed many of the generic issues based upon an earlier (20 year duration) state estimate. Results in that paper are focussed on removal of the apparently deterministic ocean circulation structures by way of a singular vector analysis, and the separation of stochastic and systematic errors in the system, prior to calculations of the uncertainties of the time-means. Although the goals of this present paper are basically the same as in W18, a different statistical methodology is employed, one focussed more directly on the nature of the multi-decadal time variability in the state estimate and its spatial structure.

Most extant statistical estimates of oceanic (and many other) properties such as time-means, trends, spectra, are based upon important default assumptions about the time series of properties. That they are: (A) Statistically stationary; (B) Gaussian or at least unimodal; (C) Have an uncertainty computable from a simple variance, or autocovariance (Gauss-Markov) estimate. Understanding of the reliability of those assumptions underlies understanding of ocean/climate change.

The approach taken here has a context of the time series analyses in several textbooks (e.g., Brockwell and Davis, 1991, Beran, 1994, Chatfield, 2004, Box et al., 2008) that are directed at understanding the import of deviations from (A), (C), and with brief examinations of (B). Underlying these discussions are the descriptors commonly known as autoregressive moving average processes (ARMAs) for linear time series, extended to account for non-stationarity as autoregressive integrated moving average processes (ARIMAs). Brockwell and Davis (1991) and Beran

(1994) have specific discussions of the ambiguities arising both from non-stationarity, and the specific behavior of the autocorrelations in stationary processes. Percival et al. (2001), Percival and Rothrock (2005), Overland et al. (2006), Gil-Alana (2012), Gil-Alana et al. (2022) among others provide more familiar climate-change related discussions of these processes. Dangendorf et al (2014) describe long-memory components in the altimetric record. Mudelsee (2001) is a textbook with applications to climate.

To some degree, the story here is a simple cautionary one—time series and the uncertainties of their properties such as the time means and trends, have a strong regional variations, ones that must be accounted for in discussions of global averages, of changing climate, or predictions. Apart from the statistical consequences, the specific results here can be understood as an unorthodox, but useful, descriptive oceanography of the characteristics of global temporal variability. An underlying issue is the extent to which discussions of global average climate physics are a substitute for potentially radically different behavior in different regions.

Consider the best linear unbiassed estimate (BLUE) estimate of an average, familiar in oceanography as arising from the Gauss-Markov theorem (e.g., Wunsch, 2006, P. 133) and the Yule-Walker equations. Let, $\xi(\mathbf{r},t)$, be a *stationary Gaussian* time series at unit time step, Δt. (Here $\mathbf{r}$ are the position coordinates and t is time. All variables are discrete.) Let its temporal autocovariance be denoted $\varphi_{\xi\xi}(\mathbf{r},\tau) = \langle \xi(\mathbf{r},t)\xi(\mathbf{r},t+\tau)\rangle$ taken about the true process mean, here assumed zero, the bracket denoting statistical expectation and estimated as $\tilde{\varphi}_{\xi\xi}(\mathbf{r},\tau) = 1/N\sum_{j=0}^{N-1}\xi(\mathbf{r},j\Delta t)\xi(\mathbf{r},(j+\tau)\Delta t)$ at lag τ, over N samples. (A tilde is used throughout to denote an estimate.) Define $\mathbf{R}_{\xi\xi}$ as the Toeplitz matrix of $\varphi_{\xi\xi}(\mathbf{r},\tau)$ for fixed $\mathbf{r}$, and discrete τ_n. Then an estimate of the true mean is the sample mean,

$$\bar{\xi}_{GM} = \frac{\mathbf{D}^T\mathbf{R}_{\xi\xi}^{-1}\boldsymbol{\xi}}{\mathbf{D}^T\mathbf{R}_{\xi\xi}^{-1}\mathbf{D}} \tag{1}$$

where $\mathbf{D} = [1,1,...,1]^T$ and ξ is the ordered column vector of all of the individual values in time. The uncertainty of $\bar{\xi}_{GM}$ about the true mean is,

$$\tilde{\sigma}^2 = \frac{1}{\mathbf{D}^T\mathbf{R}_{\xi\xi}^{-1}\mathbf{D}} \tag{2}$$

(If $\xi(\mathbf{r},t)$ are independent white noise processes, both these expressions reduce to the conventional simple average and its variance.) A central assumption is that for large τ, $\varphi_{\xi\xi}(\mathbf{r},\tau) \to 0$, rapidly, defining a "short-memory" process. Behavior of the autocovariance at large lags determines the statistical reliability of any such estimates of time-means or apparent trends. If the autocovariance fails to diminish sufficiently rapidly, the value of $\tilde{\sigma}$ in Eq. (2) is no longer accurate and can be a gross underestimate of the true uncertainty of the sample mean.

In much of the literature, commonly directed at econometric time series, processes with values of $\varphi_{\xi\xi}(\mathbf{r},\tau)$ that diminish too slowly in τ for the validity of Eq. (2) and other quantities are called "long memory processes." "Long memory" does *not* refer to the physical memory. Instead, it is a descriptor of processes whose autocovariances/autocorrelations decay sufficiently slowly so as to render inaccurate, sometimes grossly so, calculated means, trends and other estimates. One mechanism by which long memory arises naturally (Granger, 1980, Beran, 1994) comes from the summation into a physical variable of underlying independent processes of short memory. The concept is widely used in econometrics. That oceanic variations at a point are indeed at least in part the result of summations of fluctuations, perhaps independent, arriving from globally distributed distances is hardly in doubt. Whether they depict "long memory" behavior has to be determined. For purposes of this paper, "long memory" in the econometric sense will be labelled "long-autocovariance memory", to distinguish it from "long-physical memory", the latter based upon the various physics of the sort depicted in Fig. 1. Long-physical memory will be identified with the non-statistically stationary ocean regions. [1]

As an inverse problem solution method as practiced in ECCO, state estimation provides-in principle-a quantitative estimate of the uncertainty of the state estimate elements. In the global oceanic case, dimensionality is the overwhelming central problem. Consider that a coarse resolution ocean model (1° of latitude and longitude) with 50 layers and a complete state vector consisting of three components of velocity, temperature, salinity, and pressure) contains at each time-step approximately, $N \approx 10^7$, elements, omitting e.g., the also uncertain meteorological fields and the various turbulence and other parameters that are also estimated. Conventional state estimates employing the above assumptions, embodied in such linear algorithms as the Kalman filter, require calculation of covariances that are square of dimension N, and which lie beyond most existing computational resources. (See Kalmikov and Heimbach, 2014, for discussion of various

[1] The problem resembles some encountered in spatial epidemiology, as described e.g. by Lawson et al. (2020), Elliott et al. (2000).

approaches; and Heimbach et al. (2011) for sensitivity analyses using the adjoint solution.) Inclusion of accompanying atmospheric, cryospheric, and regional turbulence models and their state vectors makes the situation even more challenging. Ensemble methods are again—in principle–a solution, but in practice almost all ensembles have dimensions minute compared to N, leaving huge nullspaces in the range being covered.

Until such time as rigorous uncertainty estimates become available, an interim approach is needed. Consider the time-dependent state estimate here as though it were a physical ocean that one can sample and analyze—treating the underlying model physics as a black-box parameterization. Thus, for example, the surface elevation at any point, $\eta(\mathbf{r}_0, t)$, can be analyzed for its time-average, its trends if any, its variance etc. At the end of the analysis one has a useful, if unorthodox, description of important elements of the global ocean circulation. This approach does assume that the temporal and spatial variability is primarily stochastic in nature—despite the omnipresence of the governing approximation to the Navier-Stokes equations, sometimes in a deterministic setting. Much of the forcing is stochastic in nature, and with the existing resolution, no evidence has yet appeared for the presence of chaotic fluctuations.

2. Statistical Issues and Notation

A partial context for this and related discussions is the common "rednoise" behavior of the various geophysical variables with connections to fractal processes. That is, many variables of interest have power spectral densities (or equivalent periodograms) which appear to increase with increasing period—decreasing frequency, $s \to 0$. In the ocean context, rednoise spectra are very familiar, but are normally not examined closely for the physics present at the lowest accessible frequencies. A particularly interesting aspect concerns the question of what can be inferred about the influence of timescales of longer than the duration of observations or model runs? Discussion is far from straightforward. In W18 such processes were treated as though deterministic during the interval T_D—at least partially separating stochastic from systematic errors.[2]

As described in a number of textbooks (e.g.,Priestley, 1982; Brockwell and Davis, 1991; Box et al., 2008) the general machinery of ARMA (autoregressive moving average) and ARIMA (autoregressive integrated moving average) processes provides a useful framework for discussion

[2]Systematic errors in both observations and models are ubiquitous. Liu et al (2024) show the appearance of such errors in one type of observation (Argo salinities).

of many linear time series. Here the discussion is confined to developing a useful notation (Chatfield, 2004, aptly characterizes the literature as "challenging."). A somewhat more extensive summary is provided in the Appendix. What distinguishes the problem here from the textbook examples is the need to analyze a very large set of multivariable time series of interconnected, diverse, statistical distributions. Only a limited exploration of those statistics is undertaken.

Consider a discrete-in-time series at spatial point $\mathbf{r}$, and discrete time t with time-step $\Delta t = 1$. Let B denote a backwards in time operator:

$$B\xi(\mathbf{r},t) = \xi(\mathbf{r},t-1). \tag{3}$$

Then if $\xi(\mathbf{r},t)$ is a stationary, causal, linear process, its time evolution can be described accurately in the ARMA(p,q) form,

$$\phi(B)\,\xi(\mathbf{r},t) = \psi(B)\,\varepsilon(\mathbf{r},t) \tag{4}$$

where $\phi(B) = 1 - \phi_1 B - \phi_2 B^2 - \ldots \phi_p B^p, \psi(B) = 1 - \psi_1 B - \psi_2 B^2 - \ldots - \psi_q B^q$ are polynomials in B, of order p,q respectively, and $\varepsilon(t)$ is a white-noise (uncorrelated) random process. Polynomial coefficients, ϕ_j, ψ_j are all functions of $\mathbf{r}$ and are generally expected to be well-behaved (in particular, to be of finite length or rapidly convergent). A great deal is known about methods for estimating p,q and their reliability.[3]

As much of the literature emphasizes, it is rare to be able to assert that any particular estimation-derived model is "correct"—only that it proves useful—e.g., in description or prediction. In the oceanic problem, one normally assumes that an extended form of the Navier-Stokes equations must describe the fluid behavior. The availability of known underlying physics represents an important contrast with econometric problems. In practice however, the physics equations are always approximated to a significant extent, producing major empirical elements analogous to the purely empirical econometric ones.

Let,

$$\hat{\xi}(\mathbf{r},s) = \sum_{t=0}^{N-1} \xi(\mathbf{r},t)\, e^{-2\pi i s t} = \sum_{t=0}^{N-1} \xi(\mathbf{r},t)\, z^t,\ z = e^{-2\pi i s}, \tag{5}$$

[3]The system can be generalized to vector fields $\boldsymbol{\xi}(t)$, with the polynomial coefficients ϕ_i, ψ_i becoming matrices. Brockwell and Davis, (1991, Ch. 11) discuss such multivariable MARMA. Extension to MARIMA processes does not appear to have been widely explored apart, surprisingly, in studies such as tourist distributions (Goh and Law, 2002). Beran et al. (2013, P. 76) provide references to the financial literature.

be the Fourier transform of $\xi(\mathbf{r},t)$, starting at $t=0$ and extending to N observations (and it is a polynomial in z, the z-transform). Then the periodogram is defined as,

$$P(\mathbf{r},s_n) = |\hat{\xi}(\mathbf{r},s_n)|^2,\ s_n = \frac{n}{N}. \tag{6}$$

The power spectrum, $\Phi(\mathbf{r},s_n)$ is a smoothed and scaled version of $P(\mathbf{r},s_n)$, computed so as to reduce the variance of the elements of $P(s_n)$. (The Wiener-Khinchin theorem asserts that $P(\mathbf{r},s_n)$ can be computed from the Fourier transform of $\varphi_{\xi\xi}(\mathbf{r},\tau)$ and so they have the same information content. Power spectra are commonly normalized to spectral densities to render the results somewhat insensitive to record length.) The periodogram of the ARMA(p,q) is,

$$P_{ARMA}(\mathbf{r},s_n) \sim \left(\frac{\left|\psi\left(\mathbf{r},e^{-2\pi i s_n}\right)\right|^2}{\left|\phi\left(\mathbf{r},e^{-2\pi i s_n}\right)\right|^2} \right), \tag{7}$$

for fixed $\mathbf{r}$; see Brockwell and Davis (1991, P. 377). For present purposes, the important assumption is that $P_{ARMA}(\mathbf{r},s_n)$ is a well-behaved, smooth, finite function as $s_n \to 0$. For stable polynomials, it can be confirmed that the corresponding autocovariance, $\varphi_{\xi\xi}(\mathbf{r},\tau)$, goes to zero at finite lags. Statistical stationarity requires that at $s=0$ the periodogram of $\xi(\mathbf{r},t)$, as derived from Eq. (4) or equivalent, is finite.

Much of the statistical literature is focussed on stationary processes. For *non-stationary* $\xi(\mathbf{r},t)$, a stationary representation can often be obtained by first taking a temporal difference. For example, sometimes a non-stationary $\xi(\mathbf{r},t)$ can be rendered temporally stationary by computing $w(\mathbf{r},\mathbf{t}) = \xi(\mathbf{r},t) - \xi(\mathbf{r},t-1) = (1-B)\xi(\mathbf{r},t)$ and which can be represented as an ARMA. The process is made general by finding an ARMA of $w(\mathbf{r},\mathbf{t})$, defined as,

$$w(\mathbf{r},t) = (1-B)^d \xi(\mathbf{r},t) \equiv \nabla_d \xi(\mathbf{r},t) \tag{8}$$

$$\nabla_d = (1-B)^d = \sum_{k=0}^{\infty} \frac{\Gamma(d+1)}{\Gamma(k+1)\Gamma(d-k+1)} (-1)^k B^k, \tag{9}$$

where d does *not* have to be an integer and Γ is the gamma function.

For present purposes and as sketched more fully in the Appendix, d determines the behavior of the periodogram or spectrum for the underlying variable ξ as $s \to 0$. The periodogram is (Beran,

1994, Hurvich and Ray, 1995),

$$P(\mathbf{r},s_n) \approx F(\mathbf{r},s_n) s_n^{-2d},\ s_n \to 0. \tag{10}$$

where $F(\mathbf{r},s_n)$ is assumed to be a slowly changing smooth function derived from the corresponding ARMA(p,q). $s_n = n/(N-1)\,\Delta t$ are the Fourier series frequencies. The best-fitting straight line,

$$\log(P(\mathbf{r},s_n)) = \beta_0(\mathbf{r}) - 2d(\mathbf{r}) \log(s_n) + \hat{\varepsilon}(\mathbf{r},s_n), \tag{11}$$

provides an estimate of $d(\mathbf{r})$ where $-2d(\mathbf{r})$ is the slope of the logarithm of the periodogram or power density, over a limited band of log frequencies close to $s = 0$. $\hat{\varepsilon}(\mathbf{r},s_n)$ is a residual being minimized in the mean-square and is preferably a white noise process. In the present context, determination of $d(\mathbf{r})$ for time series in the variables of the state estimate serves several purposes. It is a spatially varying: (A) Description of the low oceanic frequencies (e.g., rednoise, blue noise, etc.). (B) An indicator of statistical stationarity or otherwise. (C) A measure of the differing spatial variability regimes permitting averaging and trend determination in statistically homogeneous terms.

In the present context, stationarity versus non-stationarity has important physical meanings: The Navier-Stokes equations are believed to be causal, and thus in principle their solution (the state) is dependent upon initial conditions. To the extent a time series at $\mathbf{r}$, $\xi(\mathbf{r},t)$ is found to be stationary, it represents a statistical equilibrium state, no longer evolving according to those initial conditions because of diffusion or the generation of a chaotic regime. If, on the other hand, $\xi(\mathbf{r},t)$ is found to be non-stationary, implying a continued dependence upon initial conditions preceding the interval T_D, for example, from some long-ago meteorological cold-spell or wind-shift. Another possibility is that some internal process has not reached equilibrium—e.g., an upgradient turbulent flux still undergoing adjustment.

Use of the periodogram (equivalently, the power density spectrum) for determining d is not necessary—with known alternative tests being based upon the autocovariance. But with the large variety of physics present in the ocean, the frequency domain usually produces a more immediate physical interpretation. For $d < 0$ in Eq. (10) the power is diminishing with diminishing frequency (blue noise) and conversely, if $d > 0$, the result is rednoise and implying a singularity at $s = 0$ in

$d = H - 1/2$	$H = d + 1/2$	**Character**
$0 \le d \le 1/2$	$1/2 < H < 1$	Stationary, long memory
0	$1/2$	Stationary white noise
$-1/2 \le d \le 0$	$0 \le H \le 1/2$	Stationary, finite $P(0)$,short memory
$d \le -1/2$	$H < 0$	Stationary
$d \ge 1/2$	$H \ge 1$	Non-stationary

TABLE 1. General behavior of a time series for a given value of d. H is the Hurst parameter. Various assumptions apply to the p,q polynomials. Stationarity implies a local statistical equilibrium not dependent upon earlier initial conditions, while non- stationarity likely means that dependence is still present in the ocean. Discussion can be found in Beran (1994), Chatfield (2004), Box et al. (2008) and elsewhere.

the complex frequency domain. In the interval, $0 < d(\mathbf{r}) < 1/2$, $\xi(\mathbf{r}, t)$ is both stationary and has long- autocovariance memory in the econometric sense. See Table 1. (Note that $H = d + 1/2$ is called the Hurst parameter, deriving historically from hydrology and the ancient behavior of the Nile River.) Global maps of $d(\mathbf{r})$ are here being regarded as part of the basic description of the oceanic general circulation.

In some variables of interest (e.g., surface height, heat content) the annual cycle can be quite prominent and is of interest in its own right; see Ponte et al. (2024) for a discussion of the oceanic annual cycle. It is readily removed *a priori*, albeit the ARIMA estimation machinery can detect such behavior—if not anticipated. Here, the values of the periodogram at periods shorter than 2.6 years are not used and the annual cycle is ignored or suppressed in what follows.

It is important to note that d, as well as any p, q, will be estimated values, written as $\tilde{d}, \tilde{p}, \tilde{q}$, each with a corresponding uncertainty. A rigorous understanding of the uncertainty e.g., of a linear trend in the presence of multiple physical processes, is a formidable task. A form of bootstrap Monte Carlo strategy will be used below (see e.g., Mudelsee, 2014, for examples).

Means, Variances, Trends

For Gaussian white noise, $\varepsilon(t)$, Eqs. (1, 2) for the the sample mean and its variance reduce to,

$$\bar{m} = \frac{1}{N} \sum_{0}^{N-1} \varepsilon(t), \tag{12}$$

$$\bar{\sigma}^2 = \frac{1}{N}\sum_{0}^{N-1}(\varepsilon(t)-\bar{m})^2 \to 0,\ N\to\infty, \tag{13}$$

the conventional mean and variance. (A fixed position $\mathbf{r}$ is implicit.) Modifications such as the Gauss-Markov estimate are readily made for processes having finite autocovariances (Eqs. 1, 2). The main point is that the variance diminishes with $1/N$, $N\to\infty$, in these cases. If however, a process $\xi(\mathbf{r},t)$ is an ARIMA(p,d,q), $-1/2 < d < 1$, then, Brockwell and Davis (1991, P. 527), the variance about the sample mean is,

$$\bar{\sigma}^2 \to \frac{C}{N^{1-2d}}, \tag{14}$$

where C is a finite constant, having potentially much slower convergence with N for $d > 0$ than is the value in Eq. (13). With $d = 1/2$, the variance does not diminish with N for large N. ($d = 1/2$ corresponds to a random walk in $w(\mathbf{r},t)$ and which has a variance increasing with time).

Determining global changes and trends in quantities such as heat content involves computing a global spatial average through time. A global average can always be computed, either directly or one whose elements are weighted as in Eq. (1) where the weights are known. Spatial variations in $\tilde{d}$, if they exist, imply that the simplest spatial averaging method, generally used also for directly observed data (e.g., temperature from CTDs) is averaging "apples and oranges"—stationary and non-stationary, long- and short-autocovariance memory, and those from regions subject to long-physical memory time series.

3. Spectral Behavior of ECCO(v4r4)

a. Sea Surface Height

Consider as a first example the behavior of the sea surface height, $\eta(\mathbf{r}_i,t)$, estimated as monthly averages, producing 312 samples at $\Delta t = 1/12$year for 26 years (and see the corresponding discussion in W18). $\mathbf{r}_i$ is the collection of two-dimensional grid positions and t is discrete. Unless otherwise stated, spatial resolution is 2° in longitude, 1° in latitude (model grid resolution is significantly higher). A plausible, greatly simplifying, physical interpretation is that with the existing spatial resolution, η, is dominated by the surface geostrophic flow. Measurements from the series of altimetric satellites make it the most uniform and spatially dense of all of the observation types to which ECCO(v4r4) was fit. Dominance (mostly) of thermal wind balance over the bulk of the

ocean also suggests that treating it as a linear variable is also a useful approximation. The ordinary time-averaged map from a shorter interval, $\bar{\eta}(\mathbf{r}_i)$, can be seen in Wunsch (2024), and is generally oceanographically conventional in the magnitude and shape of the spatial structures. Hughes and Williams (2010), Xu and Fu (2012) display estimates of the complicatd spatial structure of the frequency spectral density from altimetric data.

Fig. 2 shows not untypical monthly time series at various latitude points along 180°W in the Pacific Ocean. Visually, weak (relative to the variations) trends appear and as discussed e.g., by Percival et al. (2001), one confronts the question as to whether the trend is a stochastic accident of these times and places, or whether it represents the externally deterministic global warming consequences—a conundrum of finite T_D. In some locations, the annual cycle is prominently visible in the variability.

In what follows, the discussion of $\eta(\mathbf{r},t)$ is restricted to the region equatorward of 60^oN and 65°S to avoid the complexities of determining sea level change in the presence of sea-ice. The restricted region corresponds to the coverage latitudes of the TOPEX/POSEIDON, Jason, and Sentinel series of altimetric measurements. Fig. 3 displays the histogram of the time-dependent elements of $\eta(\mathbf{r}_i,t)$ for all $\mathbf{r}_i,t$ with their time-average removed. Unimodality is clear, although a Gaussian would be only a crude approximation. The periodograms from the time series along 180°W and the global average spectra before and after removal of the annual cycle are displayed in Fig. 4.

For $\eta(\mathbf{r},t)$, the presence of a trend owing to global warming is plausible in many regions, but whether it is visible in all regions is much less clear. For that reason, the analysis here is carried out twice: (1) With the full value of $\eta(\mathbf{r},t)$, and (2) with $\tilde{\eta}(\mathbf{r},t)$ from which a linear time trend has been removed at each grid point by conventional, unweighted least-squares. In the statistical context, the linear trend is then being assumed to be an externally imposed deterministic forcing; although given the multiplicity of causes of sea level change, its existence and magnitude is a potentially strong function of position.

The area weighted average of $\tilde{\eta}(\mathbf{r},t)$ is depicted in Fig. 5. Based on this result it is concluded that representation of the overall trend by a straight line is adequate at this stage of understanding. (In contrast, Cazenave and Moreira, 2022, conclude that deviations from a linear rule are detectable.) Fig. 6 shows the average of η at year 26 minus that from year 1, producing a spatial average of 0.0016 m/year=1.6mm/y or 4 cm over 26 years—with an uncertainty discussed below. Fig. 7

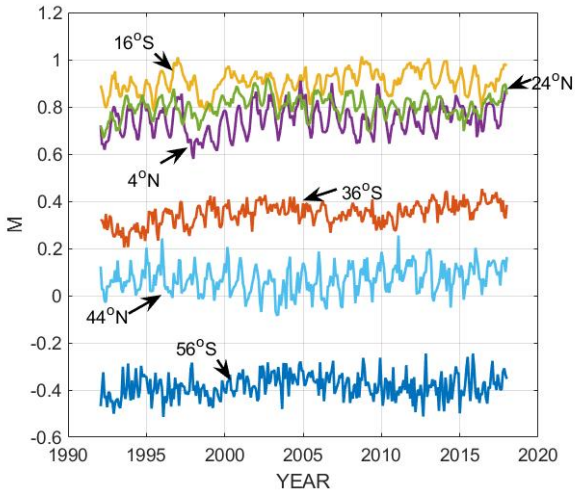

FIG. 2. Representative time series of $\eta(\mathbf{r},t)$ along 180°W in the central Pacific Ocean. The qualitative change with latitude is clear. A visible annual cycle exists at some latitudes and has generally been suppressed in the analysis here.

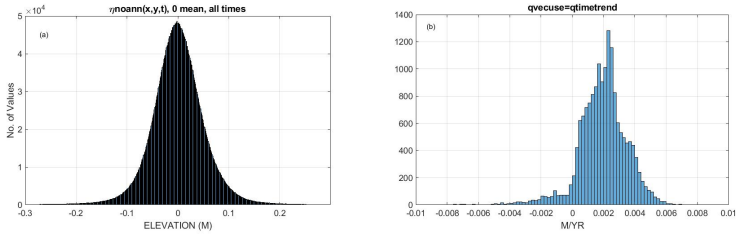

FIG. 3. (a) Histogram of $\eta(\mathbf{r}_i,t)$ with local time averages and the annual cycle removed for all times and positions. A unimodal description is accurate, and a Gaussian is a plausible first approximation. A small number of extreme outlier values are omitted here. (b). Histogram of estimated values of $\Delta\eta/\Delta t$ and which is non-Gaussian. An excess of positive values is apparent. Bootstrap values are drawn from this distribution, which varies with $\tilde{d}$.

displays the estimated sea level height trend, $\Delta\eta/\Delta t$, from the fit to $\eta(\mathbf{r}_i,t)$ over the 26 years. (The strong regionality of the temporal variability in $\eta(\mathbf{r}_i,t)$ can be seen in Xu and Fu (2012; reproduced in Wunsch and Heimbach, 2016), rendering complex the determination of the uncertainty of the

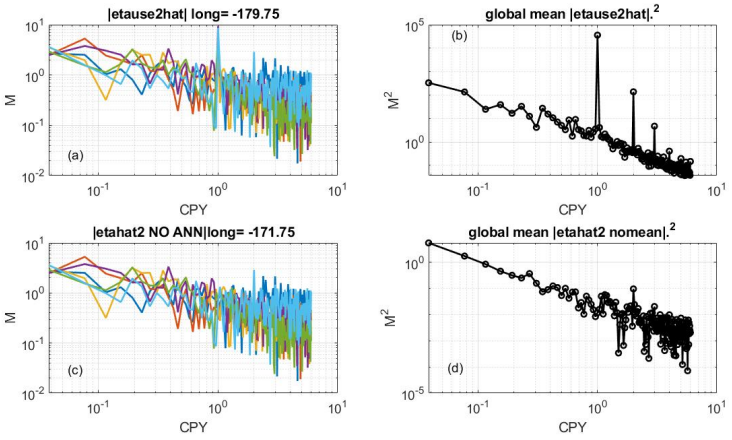

FIG. 4. (a) Periodogram estimates of $\eta(\mathbf{r},t)$ at points along 180°W in the central Pacific Ocean and (b) the global average of the $\eta(\mathbf{r},t)$ periodograms showing the prominence of the annual peak. (A secondary peak appears at 6 mos. period, but is being ignored.) (c) Periodograms without the annual cycle along 180°W and (d) the global average of all periodograms without annual cycles. First 10 periodogram frequencies are used to determine $\tilde{d}$.

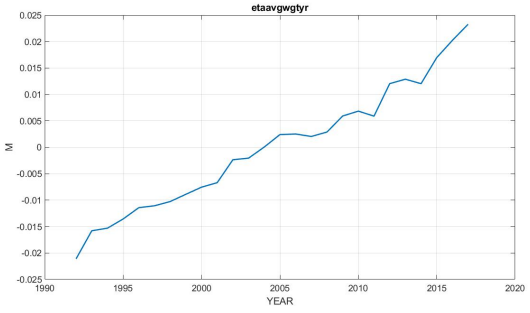

FIG. 5. Spatial average of the area-weighted value of $\tilde{\eta}(\mathbf{r},t)$ for each of 26 years in the latitude range depicted in Fig.6. An issue, not addressed here, is whether deviations from a straight line are significant.

slope, and which is taken up below.) A few regions of negative slope (falling sea level) are apparent. Cazenave and Moreira (2022) review previous estimates of sea level rise and report a global trend from 1992 to 2022 of 3.33 ± 0.33mm/y, where the uncertainty is intended as a 90% confidence interval (but see Lanzante, 2005; Ambaum, 2010). That Fig. 6 has more structure than Fig. 7 is an indication of the noisiness in any particular one-year average relative to that of the entirety of T_D. (The W18 value was based solely upon the difference of the average in the first and last years, as a way of eliminating systematic errors in the state estimate.) Apart from the extreme positive values

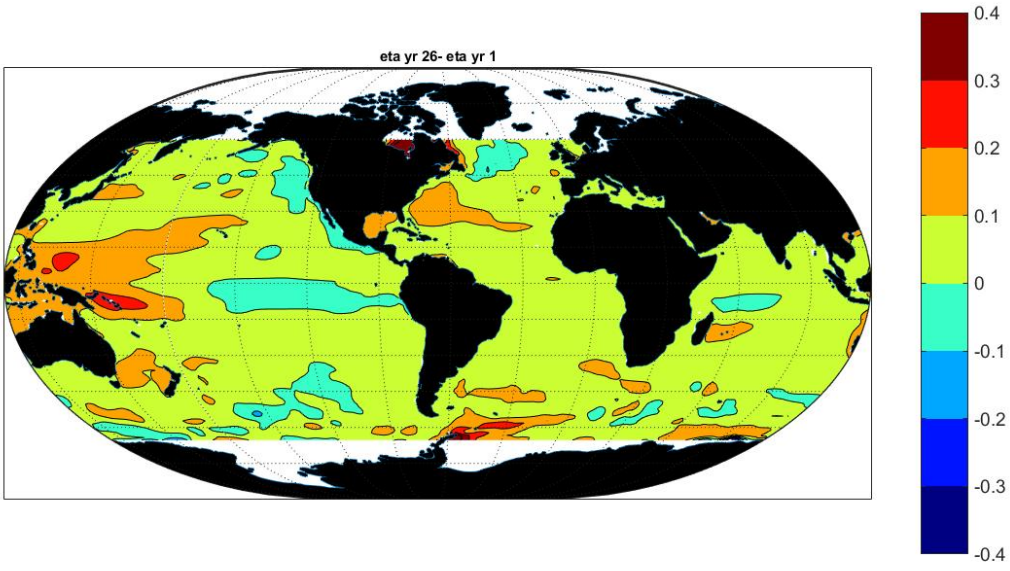

FIG. 6. $\eta(\mathbf{r}_i, t)$ (in meters) averaged over year 26 minus the same average over year 1. Generally positive values dominate. As argued in W18, this difference will tend to be insensitive to systematic errors, although each averaged year (not shown) is noisier than the average over all T_D. The spatial structure hints at the observational sampling issues.

in the Arctic Seas (not shown), a few comparatively small regions, particularly in the Southern Ocean, appear to have declining sea level. Like the Arctic Seas, the immediate regions of the Antarctic continent are strongly affected by sea ice cover. Otherwise, a nearly uniform increase in sea level of about 1.5mm/y is seen over the bulk of the global ocean and its spatial simplicity, a contrast with most other oceanic fields, strongly suggests causation by externally imposed physics.

If a best fit is made to the logarithms of the periodograms (Eq. 11) of $\eta(\mathbf{r}, t)$ for the 10 frequencies lying between 1 cycle/26 years, and 1 cycle/2.6 years, the resulting value of $\tilde{d}$ can be seen in Fig. 8. With the use of only 10 frequencies, the uncertainty in $\tilde{d}(\mathbf{r})$ is substantial. Emergence of large regions of nearly constant $\tilde{d}$ provides some reassurance as to the robustness of the result; that the variability in these regions is not independent must however, also be kept in mind.

Much comparatively small spatial scale structure emerges, and perhaps calling for spatial smoothing—given that $\tilde{d}$ is only an estimate of the true value. This and other figures are left unsmoothed to give some impression of the noisiness even of a 26 year temporal average. Among

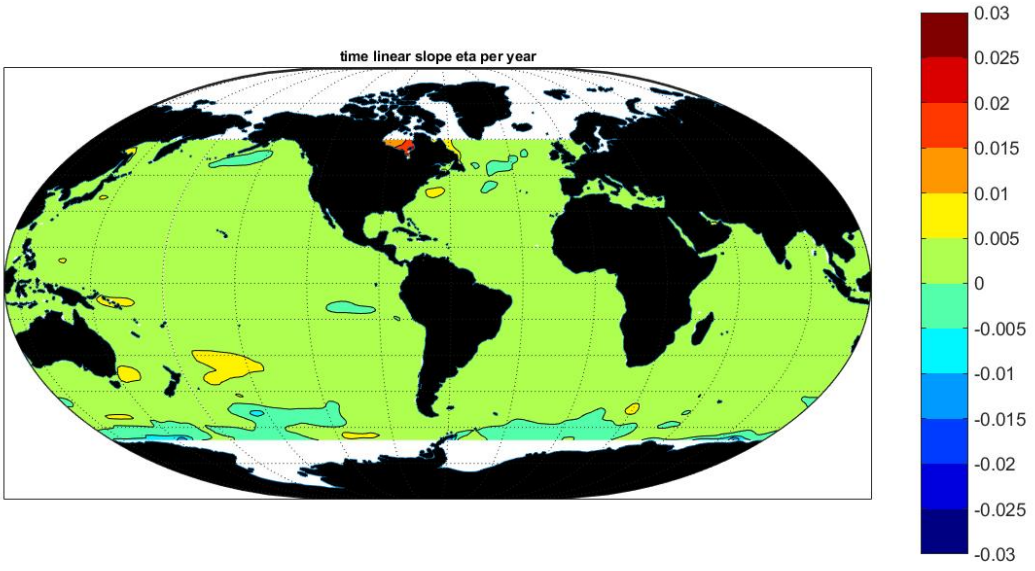

FIG. 7. Best fitting (ordinary least-squares) estimated linear trend, $\Delta\eta(\mathbf{r}_i,t)/\Delta t$, of $\eta(\mathbf{r}_i,t)$ over 26 years (M/Y). Arctic values are ignored here, as sea ice physics must be accounted for. Areal mean value is 1.6mm/y. The open ocean 26-year trend is spatially much simpler then the trend computed from two individual years.

the striking features are the east-west change in sign across the North Atlantic. It appears that the eastern North Atlantic Ocean has reached a form of statistical equilibrium, while the western portion is still responding to forcings and adjustments on time-scales exceeding T_D. Similarly the general values greater than $1/2$ in the Southern Hemisphere imply non-stationarity and long physical memory. The equatorial Pacific is notable for its negative values (blue and white noise) implying statistical equilibrium—perhaps best interpreted as owing to dominance there of the apparently stationary high frequency motions characteristic of that region. A simple, robust, inference is that the ocean circulation has a statistically very inhomogeneous behavior—an inference with direct consequences for the calculation of any global average properties, including means and trends, and a substantial area whose characteristics appear dependent upon conditions preceding the start of interval T_D. More generally, the spatial inhomogeneity of sea level change is well-known (e.g., Pugh and Woodworth, 2014), although much that has been documented lies in shallow and coastal waters—not well represented here.

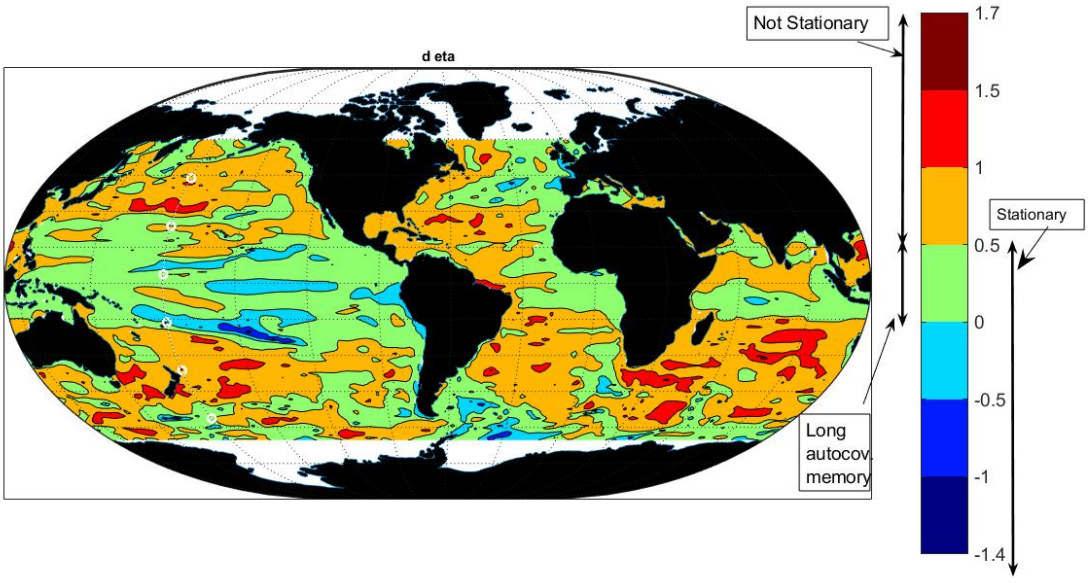

FIG. 8. Estimated $\tilde{d}(\mathbf{r})$ for $\eta(\mathbf{r},t)$ (dimensionless). Blue-green boundary corresponds to $\tilde{d}=0$, white noise behavior near $s=0$. For $0 \le d \le 1/2$, the local process has long-autocovariance memory. For $d < 1/2$ it is stationary and for $d > 1/2$ not stationary. White circles indicate positions of time series in Fig. 2 along 180°W. The east-west structure in the North Atlantic Ocean remains.

When the linear in time trend at each point (Fig. 7) is removed first, the result, $\tilde{d}_{NS}$, is shown in Fig. 9 and which, as expected, differs from $\tilde{d}$. Rapid changes in sign occur across the equator in the Pacific, with the North Atlantic still showing an east-west shift between stationary and non-stationary areas. Apart from the Agulhas region, the Southern Ocean presents a very noisy set of values, at least qualitatively consistent with the intense structure there in all of the physical state elements (Wunsch, 2024, 2025). Whether $\tilde{d}$ or $\tilde{d}_{NS}$ is employed, it is apparent that averages taken over the global ocean involve extended regions where the underlying statistics are either not stationary, or have a long-autocovariance memory. Averages in such regions are thus anticipated to produce values whose uncertainties are potentially much greater than those derived from conventional variance and confidence limit analyses.

Standard Errors in $\eta(\mathbf{r}_i,t)$

The spatial variations in the statistical behavior embedded in $\eta(\mathbf{r}_i,t)$, do not include the variations which would appear additionally if the full ARIMA and its uncertainties were determined at each

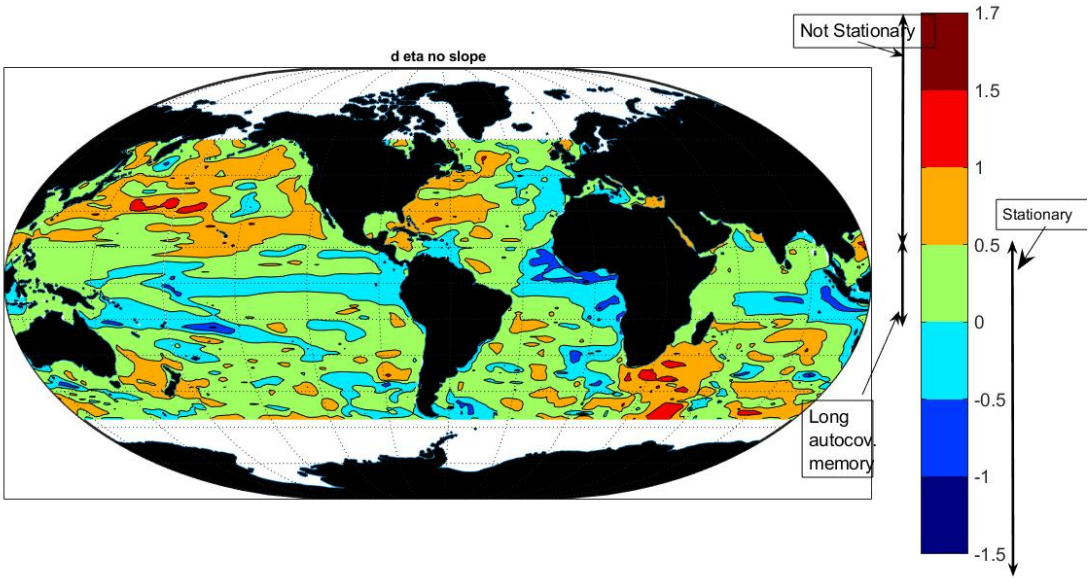

FIG. 9. Estimated $\tilde{d}_{NS}$ for $\eta(\mathbf{r},t)$ after a linear time trend is removed first.

position $\mathbf{r}_i$. Precisely how to best determine, in practice, the uncertainty in the average value of $\Delta\eta/\Delta t \approx \partial\eta(\mathbf{r}_i,t)/\partial t$ quoted above is not so clear.

As a preliminary, plausible, approach, a bootstrap (Efron and Tibshirani, 1993) is applied to the vectors composed of values of $\Delta\eta(\mathbf{r}_i,t)/\Delta t$ and the implied underlying probability density in Fig. 3b, with the annual frequency energy first removed, replacing it with an interpolation from the two periodogram values immediately adjoining. In the restricted latitude band being analyzed here, estimated values of $\Delta\eta(\mathbf{r}_i,t)/\Delta t$ for 16706 grid points are used with Δt = 1month. An estimate is made for the average value of $\Delta\eta(\mathbf{r}_i,t)/\Delta t$ for an ensemble of 5000 members randomly selected with replacement from the $1 \le i \le 16706$ grid points whose overall distribution can be seen in Fig. 3b. One finds a mean of 1.5mm/y with a bootstrap standard error (one standard deviation) of 0.013mm/y, about 1/2 the Cazenave and Moreira (2022) direct estimate of the mean quoted above.

Reconciling these conflicting estimates emphasizes again the need for a full understanding of the statistics of observations and of models. And recall the omission in the present calculation of the high latitude sea ice regions. The emphasis in this present paper is on the *spatial patterns of change* rather than the global averages and so no attempt is made here to parse the numerous physics

$\tilde{d}$	Area Fraction (%)	$\overline{\Delta\eta\left(\mathbf{r}_i,t\right)/\Delta t}$	$\tilde{\sigma}$
$0 \le \tilde{d} \le 1/2$	43	1.7mm/y	0.02mm/y
$\tilde{d} < 0$	6	0.78mm/y	0.047mm/y
$\tilde{d} > 1/2$	50	0.78mm/y	0.017mm/y
All	100	1.5mm/y	0.013mm/y

TABLE 2. Estimated sea level rate of change and its standard error for selected ranges of d

.

elements and corresponding errors making up global spatial integrals computed from varying data sets and models.

In the context of understanding the 26-year state estimate, an interesting question is whether the regions of differing ranges of $\tilde{d}$ produce different rates of change? Partial results can be seen in Table 2 and which suggests variations with $\tilde{d}$ of about a factor of 2.

At each $\mathbf{r}_i$, the time series of trends $\Delta\eta\left(\mathbf{r}_i,t\right)/\Delta t$ are themselves inferred from the local time variability and thus their trends have their own uncertainty computable from an ARIMA regression against t. An analytic estimate of that uncertainty is apparently available only for regression in t for the special case $0 < d < 1/2$ (Yajima, 1988; Beran, 1994, P. 176). A bootstrap estimate could be applied to each of them with the resulting uncertainty being employed in a correspondingly weighted spatial average. In practice, application of a bootstrap to a time series necessitates use of a block method (e.g., Mudelsee, 2010) and involves a more intricate set of calculations, including the determination of appropriate block sizes, and is not dealt with here. One might thus interpret the standard errors here, $\tilde{\sigma}$, as being lower bounds.

Because the values of $\Delta\tilde{\eta}\left(\mathbf{r}_i,t\right)/\Delta t$ in Fig. 7 are comparatively uniform, an alternative to the above analysis treats the spatial average of $\Delta\tilde{\eta}\left(\mathbf{r}_i,t\right)/\Delta t$ as an externally imposed deterministic forcing and using $\tilde{d}_{NS}$. Despite the comparative uniformity of $\Delta\tilde{\eta}\left(\mathbf{r}_i,t\right)/\Delta t$, making the case that its value is determined by a spatially uniform forcing is not so easy—given the collection of external influences on sea level, including atmospheric heating and load, wind forcing, glacial and landwater inputs, gravity changes, etc. and the ability of the ocean to transport properties over long distances. The issue is left at this point.

4. Abyssal Heat Uptake

Along with sea level change, wide interest lies in determining the rate at which heat is being absorbed by the ocean—as part of the physics of global warming. Liang et al. (2017) described the patterns and physical mechanisms of oceanic heat transport in an earlier ECCO release (v4r1), with many useful references, particularly as they relate to regional changes and they emphasized the need for global analyses. The physics of changes in the distribution of oceanic heat content are, as compared to the surface elevation in a quasi-geostrophic balance, far more diverse and complex. Assumptions such as a quasi-linear physics are more difficult to support.

Here, the goal is restricted to making an illustrative estimate of the patterns and rates of the global change in oceanic heat content, along with an illustrative estimate of its accuracy. Initially the calculation is restricted to the abyssal ocean, defined as that lying below 2000m (approximately 1/2 the ocean volume) and with estimated heat content in J m^3 most simply defined as,

$$Q_a(\mathbf{r},t) = \rho_0 c_p \Delta A(\mathbf{r}) \int_{-h(\mathbf{r})}^{-2000} \theta(\mathbf{r},z,t)\, dz \tag{15}$$

where θ is potential temperature, ΔA is the area represented by any particular grid point, ρ_0 = 1038kg/m^3, c_p = 3994J/ kg/°C. An estimate from a previous state estimate can be found in Wunsch and Heimbach (2014) and which includes discussion of the substantial observational issues. (Some published estimates of heat content are computed for the amount lying below an isopycnal. That compounds the uncertainty calculation problem by introducing another computed, partially stochastic, field—the isopycnal depth—into the upper integration limit in Eq. (15).)

The analysis generally follows that laid out above for $\eta(\mathbf{r},t)$. A histogram of all abyssal heat content values at all times is in Fig. 10, and is evidently non-Gaussian. The time average of $Q_a(\mathbf{r},t)$ can be seen in Fig. 11 with the relative warmth of the North Atlantic Ocean corresponding to its excess salinity. Time series of values in the Pacific and Atlantic along two fixed longitudes are displayed in Fig. 12. Changes relative to the time means are evidently very subtle, and their determination is part of the observational challenge in the presence of topography. A surprising amount of annual cycle energy persists at these depths almost everywhere, but is particularly pronounced in the equatorial Pacific and Indian Oceans (not shown). Any quasi-barotropic or

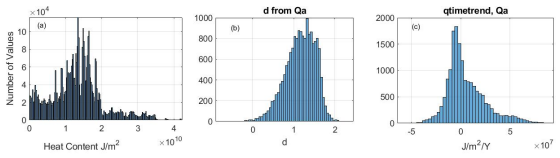

Fig. 10. (a) Abyssal heat content value distribution, all positions and all times. A unimodal description is evidently very approximate. (b) Estimated value $\tilde{d}$ for abyssal heat content; not area weighted. (c) Distribution of values of $\Delta Q_a(\mathbf{r}_i,t)/\Delta t$ and which is unimodal but skewed toward positive values. Used for the bootstrap sampling.

low vertical mode annual variability induced in the flow field will, in the presence of topography, generate an annual thermal signal at depth along with other abyssal noise processes.

The ordinary least-squares temporal trends of $Q_a(\mathbf{r},t)$ are mapped in Fig. 13 and which correspond coarsely to previous published descriptions—with the Southern Ocean abyss showing distinct warming, the bulk of the Pacific Ocean as cooling, and the Atlantic has a small region of decline embedded in a small overall increase. More structure exists as compared to the $\Delta\eta(\mathbf{r}_i,t)/\Delta t$ discussed above—consistent with the greater variety of physical processes controlling oceanic temperatures.

$\tilde{d}$ is mapped in Fig. 14. With no trend in time removed from Q_a, the abyssal heat content change is an amalgam of primarily non-stationary processes, with a very small area of long and short memory processes. Correspondence to the trends in Fig. 13 is not obvious.

Fig. 15 show the corresponding estimated values of $\tilde{d}_{NS}$. Again the intense small scale structures are the dominant feature and they have a striking resemblance to $\tilde{d}$ in the Atlantic Ocean, consistently between approximate latitudes 42°N and 15°S in being non-stationary, becoming stationary west and south of Cape Agulhas. Nonetheless, in contrast, the tropical Pacific Ocean shifts from being non-stationary, to having negative values of $\tilde{d}_{NS}$. One interpretation is that the apparent cooling in that region is the result of external forcing (e.g., the Little Ice Age; See Gebbie and Huybers, 2019),

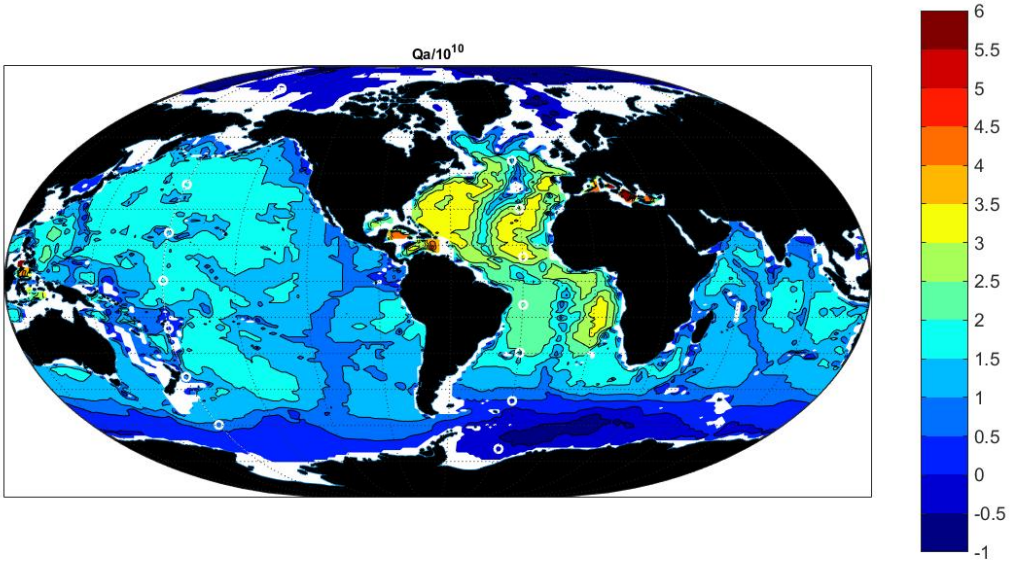

FIG. 11. Estimated time average heat content below 2000m. $\bar{Q_a}(x,y)/10^{10}$ J/m^2 . Shallower regions necessarily have less resident heat content than do deep ones. The Atlantic Ocean is strikingly warmer than the rest of the world ocean.

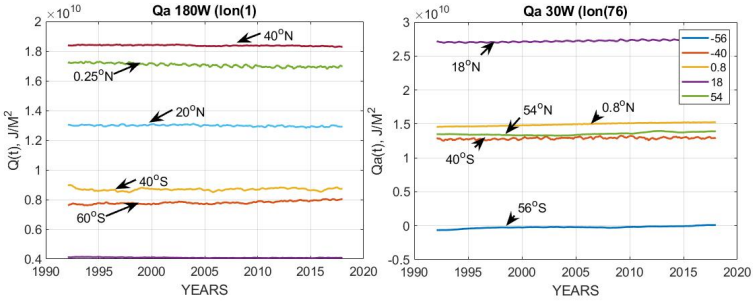

FIG. 12. (left) Time series of abyssal heat content along 180°W in the Pacific Ocean. A very small cooling—relative to the time-mean values—is visible in some places. Values are Joules/m^2. (right) $Q_a\,(\mathbf{r}_i,t)$ at positions along 30°W in the Atlantic Ocean.

with the underlying variability being dominated by high frequencies, consistent with $\tilde{d}_{NS} < 0$. A similar change is apparent in the eastern Indian Ocean.

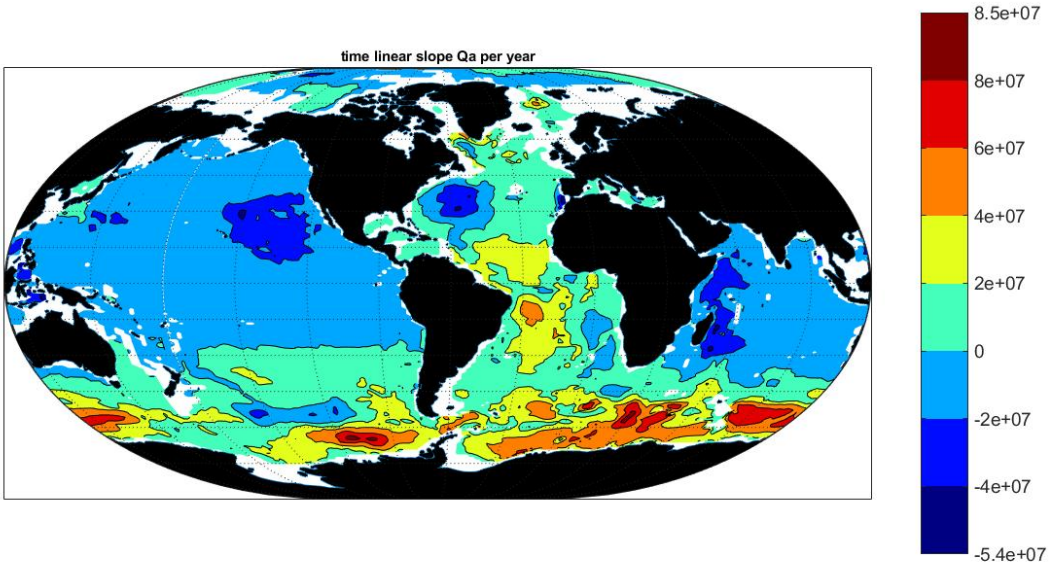

FIG. 13. Linear rate of change of the estimated abyssal heat content, $\Delta Q_a/\Delta t$ (J/m^{2}yr). Most notable is the cooling in the North Pacific and Indian Oceans, with net heating in the Southern Ocean and South Atlantic. The cooling is consistent with e.g., Gebbie and Huybers (2019) inferences concerning the ongoing role of the Little Ice Age cooling and the very long adjustment time-scales found by Wunsch and Heimbach (2008). Compare to Fig. 2 of Zanna et al. (2019) or Fig. 2 of Johnson and Purkey (2024). 10^7J/m^2/y=0.32J/m^2/s=0.32W/m^2.

The high latitude North Atlantic Ocean has very similar properties of $\tilde{d}, \tilde{d}_{NS}$, with much of the sub-polar gyre being consistent with long-autocovariance memory. A similar range of values appears in the southern regions of the South Pacific Ocean.

A priori removal of a time trend from Q_a is much less compelling that it is for $\eta(\mathbf{r}, t)$ because the the abyss is not in direct contact with the external atmospheric and radiation forcing: the physics processes leading to a change in heat content at depth are varied and only very indirectly depend upon surface boundary values.

Nonetheless, in contrast, when the linear trend of Fig. 13 is removed from the heat content time series, one perceives a distinct difference between the bulk of the Pacific Ocean and the Atlantic Ocean, with the former being dominated by stable and long-autocovariance memory processes. Much of the Atlantic Ocean remains non-stationary, with regions of intense energy growth with diminishing frequency.

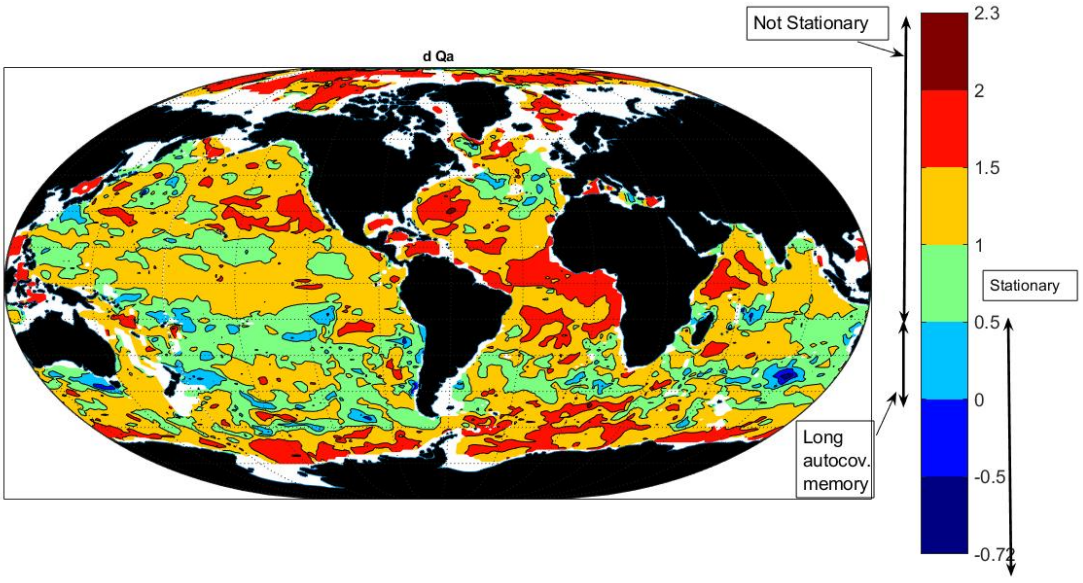

FIG. 14. Estimated exponent $\tilde{d}\,(\mathbf{r})$ for behavior of the $Q_a\,(\mathbf{r},t)$ periodogram $P \to s^{-2d}$ as $s \to 0$. Small areas of $0 \le \tilde{d} \le 1/2$ are indicators of long-autocovariance memory and larger values are non-stationary.

$\tilde{d}$	Area Fraction (%)	$\overline{\Delta Q_a\,(\mathbf{r}_i,t)\,/\Delta t}$	$\tilde{\sigma}$
$0 \le \tilde{d} \le 1/2$	5	9.2×10^5	2.7×10^5
$\tilde{d} < 0$	0.4	1.3×10^6	5.6×10^5
$\tilde{d} > 1/2$	96	5.4×10^6	1.6×10^4
All	100	5.2×10^6 J/m^{2}y	1.5×10^5 J/m^{2}2 y

TABLE 3. Estimated heat content rate of change and its standard error for selected ranges of d

The histogram of values of $\tilde{d}_{NS}$ can be seen in Fig. 10. The great bulk of the values of $\tilde{d}_{NS}$ lie between 0 and 2. About 4% of the ocean area corresponds to regions with $\tilde{d}_{NS} < 0$, where energy decreases with frequency at the low end. The spatial average time series, weighted by area, is shown in Fig. 16. Most of the heat content lies in the non-stationary areas ($\tilde{d}_{NS} \ge 1/2$).

Reference to Table 4 shows that the estimated heat uptake over the full water column is approximately twice that for the abyss alone, with approximately twice the uncertainty. Almost all of it lies in the non-stationary regions. Fig.16 displays the spatial time average of $Q_a(t)$ in three different regions of $\tilde{d}_{NS}$.

Topographic Issues

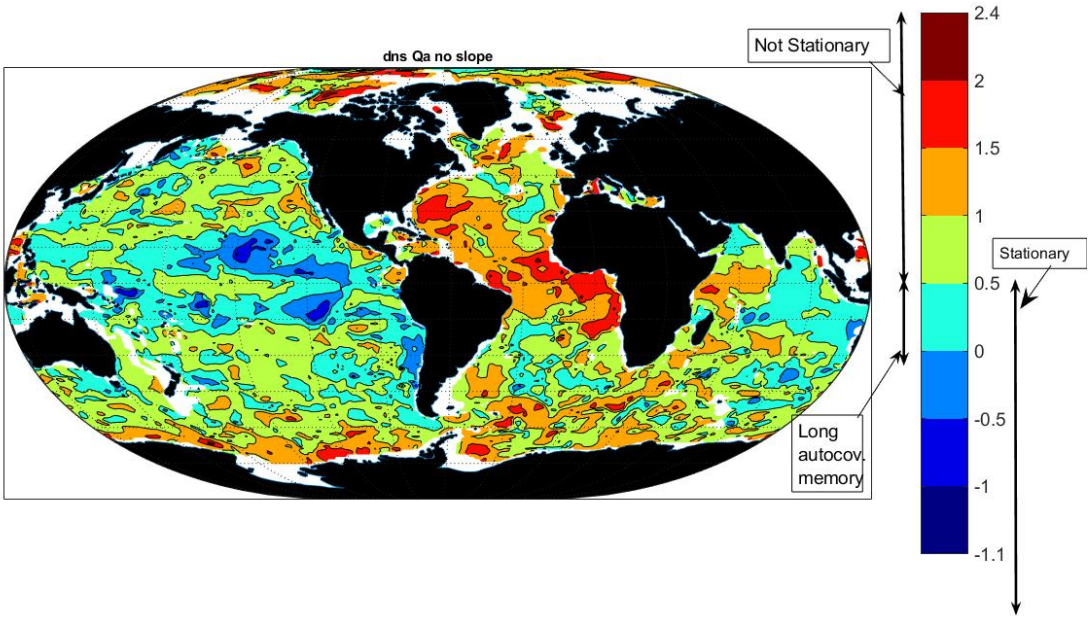

488 FIG. 15. $\tilde{d}_{NS}$ with a linear trend attributed to external causes and removed before calculation. North Atlantic,
489 its tropical regions, and much of the Southern Ocean are non-stationary and visibly different in character than than
490 elsewhere. The tropical Pacific and Indian Oceans are here dominated by stationary short-memory processes,
491 presumably including the comparatively short-lived ENSO responses.

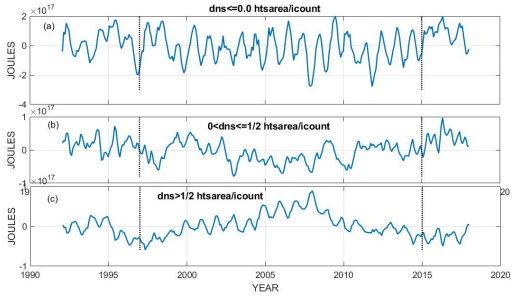

520 FIG. 16. (a) Areal average time series of heat content change Q_a when $\tilde{d}_{NS} \leq 0$ corresponding to "blue
521 noise" and visually unremarkable. (b) Space-average of area weighted region of $0 < \tilde{d}_{NS} \leq 1/2$ corresponding to
522 long-autocovariance memory. (c) Spatial average of heat content where $1/2 < \tilde{d}_{NS}$. An annual cycle component
523 of varying magnitude is visible in all three regions. Vertical dashed lines indicate years of El Nino occurrence.

525 The spatial complexity of $\tilde{d}, \tilde{d}_{NS}$ that emerges is at least in part a consequence of the very
526 complicated bottom topography of the global ocean. A claim that the model adequately resolves

the true bottom topography is difficult to sustain (deep layers in the ECCO(v4r4) version of the MITgcm have thicknesses of 400m, and a spatial resolution of order 1° does not adequately represent the details (GEBCO Compilation Group, 2024) of the known topography). Questions have even been raised about the accuracy with which the average ocean depth has been determined (Charette and Smith, 2010) although progress has been made since then using more recent satellite data. Related questions remain about the adequacy existing sampling of temperature in the deep ocean.

Totals and Bootstrap Uncertainties

The bootstrap is now applied to the abyssal heat content trends, using the different regimes of d (see Table 3). d_{NS} is not used because the relationship between the external surface exchanges and the heat content at any abyssal point is extremely indirect. The table shows a net average heating rate of 5.2×10^6J/m^{2}y or $(5.2\times10^6)/3.15\times10^7 = 0.17$W/m^2 with a one standard error of 0.005W/m^2. Zanna et al. (2019) estimated the heat uptake in the early 2000s below 2000m as 0.06±0.04W/m^2. In terms of area-integrated heat uptake the present estimate corresponds to about 20 ± 0.7TW compared to values estimated by Johnson and Purkey (2024) from Argo float and ship-based measurements, for a total of 36 ± 19TW (with the same issues concerning uncertainty estimates). Wunsch and Ferrari (2004) used an estimated total energy in the ocean circulation of 20YJ (2×10^{25}J) and so the rates of change are numerically minuscule—as would be deduced from Fig. 12 —an issue for both observation and modeling. The different values and uncertainties in these (and other) estimates rely on different sources of information and statistical assumptions. Present values are not claimed to be "correct", but merely a best estimate from the present information and assumptions.

5. Total Water Column Heat

Turning now to the total water column heat content, which includes the abyssal values as a subset, numerical values of $Q_f(\mathbf{r}_i, t)$ are dominated by the upper ocean. The observational base in approximately the upper 1000m is, although still spatially sparse compared to the highly active eddy and internal wave fields, nonetheless far improved over that available for the deep ocean. The procedures being the same as already used above, only an abbreviated discussion is provided.

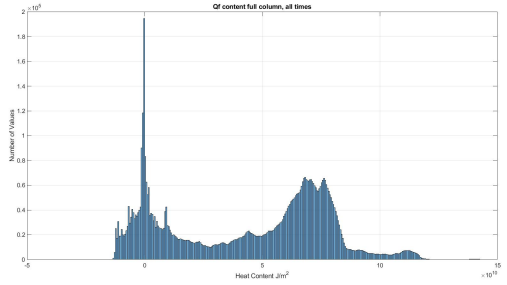

555 FIG. 17. Distribution of elements of heat content, Q_f in the full water column. Heat content in many locations
556 is small, but none actually vanishes (noting again that negative temperatures in ^{o}C produce apparent negative
557 heat content.

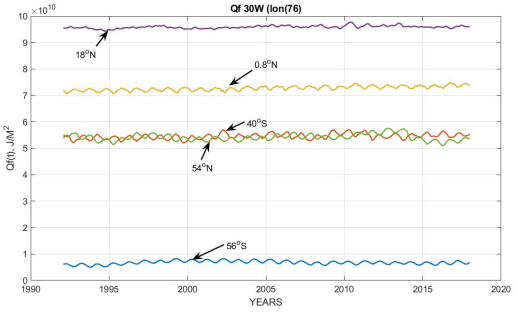

558 FIG. 18. Total heat content at various latitudes through time along 30°W in the Atlantic. Note the annual cycle
559 and its reversal in sign across the equator.

$\tilde{d}$	Area Fraction (%)	$\overline{\Delta Q_f(\mathbf{r}_i,t)/\Delta t}$	$\tilde{\sigma}$
$0 \le \tilde{d} \le 1/2$	36	1.1×10^7	3.1×10^5
$\tilde{d} < 0$	8	4.1×10^6	4.5×10^5
$\tilde{d} > 1/2$	59	3.5×10^7	4.1×10^5
All	100	2.6×10^7 J/m^{2}y	2.9×10^5 J/m^{2}y

TABLE 4. Estimated rate of change of full column heat content and its standard error for selected ranges of d

560 The distribution of heat content values can be seen in Fig. 17, and representative time series in
561 Fig. 18. As expected, a strong annual cycle is visible, one reversing in sign across the equator.
562 Calculations were done after suppressing the annual spectral energy. Fig. 19 maps the values of
563 the linear time trend and showing the complexity in the northern North Atlantic and the general
564 cooling over much of the Pacific Ocean.

573 Figs. 20, 21 show $\tilde{d}, \tilde{d}_{NS}$ for Q_f. As compared to the abyssal results, the two charts are quite
574 similar, with the tropical Pacific Ocean being a region of blue noise. The gross similarity is

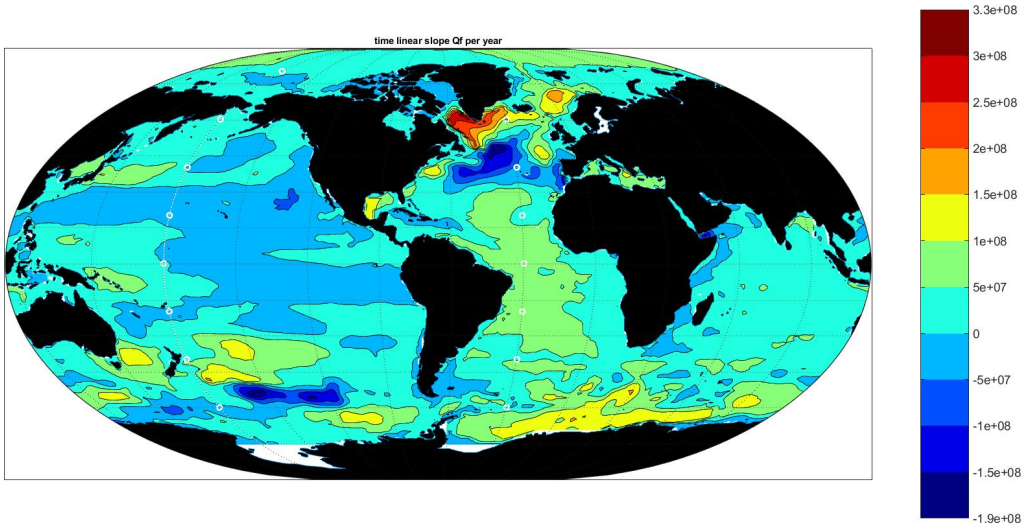

FIG. 19. Estimated linear in time trend, $\Delta Q_f/\Delta t$, for the entire water column. Complex structures in the high latitude North Atlantic Ocean are notable.

consistent with the hypothesis that the external forced, disequilibrium heating is a weak element of the fluctuations present in Q_f.

Table 4 shows the calculated global average heating for the total and by value of $\tilde{d}$. The global average total $0.83 \pm 0.01 W/m^2$, the uncertainty from the bootstrap. Because of the many elements involved in computing air-sea heat transfers, including initial conditions, and with the focus here on spatial patterns, direct comparison to other estimates is left to von Schukmann et al. (2023) and the numerous references there.

6. Discussion

From a 26-year ocean general circulation state estimate, monthly variability of surface elevation $\eta(\mathbf{r},t)$, abyssal (below 2000m) heat content, $Q_a(\mathbf{r},t)$ and total water column heat content, $Q_f(\mathbf{r},t)$ are seen to have a statistical structure which has a strong regional dependence. Forming simple spatial averages of e.g., estimated dQ/dt, to determine trends, may produce values which are strongly biassed or far more uncertain than inferred from conventional estimates.

This paper attempts to confront the spatial inhomogeneity of the time-evolving oceanic structures and to make some estimates of heat uptake and sea level rise and their uncertainties. The

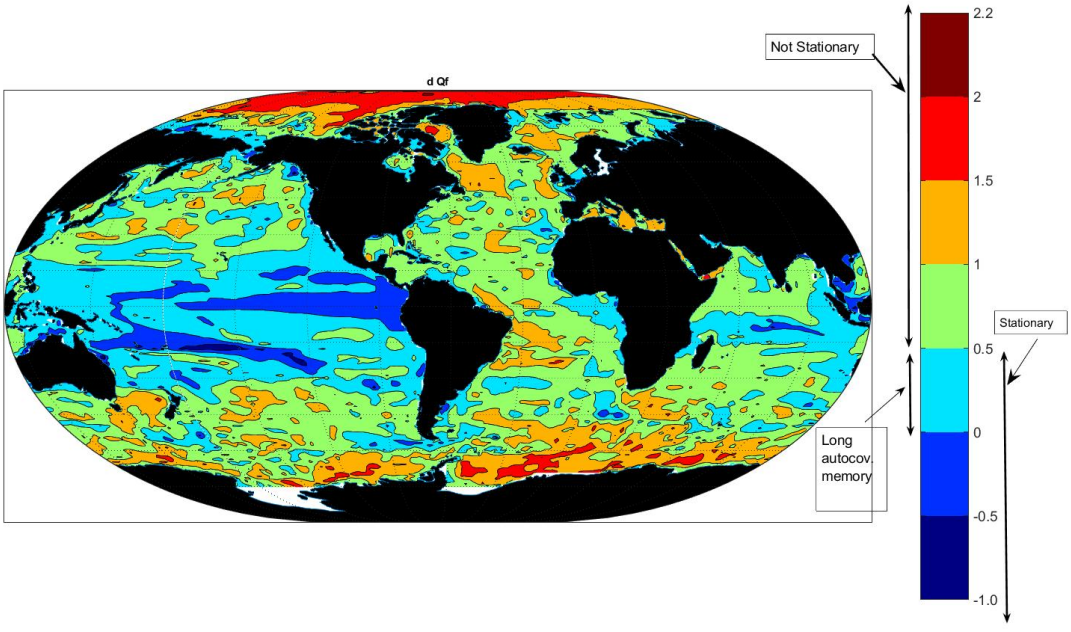

FIG. 20. $\tilde{d}$ for the total water column heat content. The South Atlantic and South Pacific Oceans differ significantly with the former having non-stationary behavior (long-physical memory) with the latter having regions of short autocovariance behavior and blue noise.

statistical structures are embedded in the formalism of autoregressive integrated moving average (ARIMA(p,d,q)) structures, with a focus on the temporal differencing parameter d. That dependence is determined from analyses of the lowest available frequencies. These differing regions are inferred to be dependent upon varying contributions from both internal adjustment time-scales (e.g., large-scale baroclinic disturbance propagation) and externally imposed forces (e.g., forced global warming elements). A definitive separation between these two sources cannot be made, and thus two different renderings of the long time-scale behaviors are made, one assuming that all the variability is internal to the system, and second assuming a linear dependence upon externally imposed global warming forcing. The most robust conclusion for the heat content is that while the global warming signature is visible over much of the ocean, many other parts are responding with long-physical memory to disturbances in the distant past, or to propagation from distant regions. For sea level change in particular, where the observations are most direct and dense, the inference

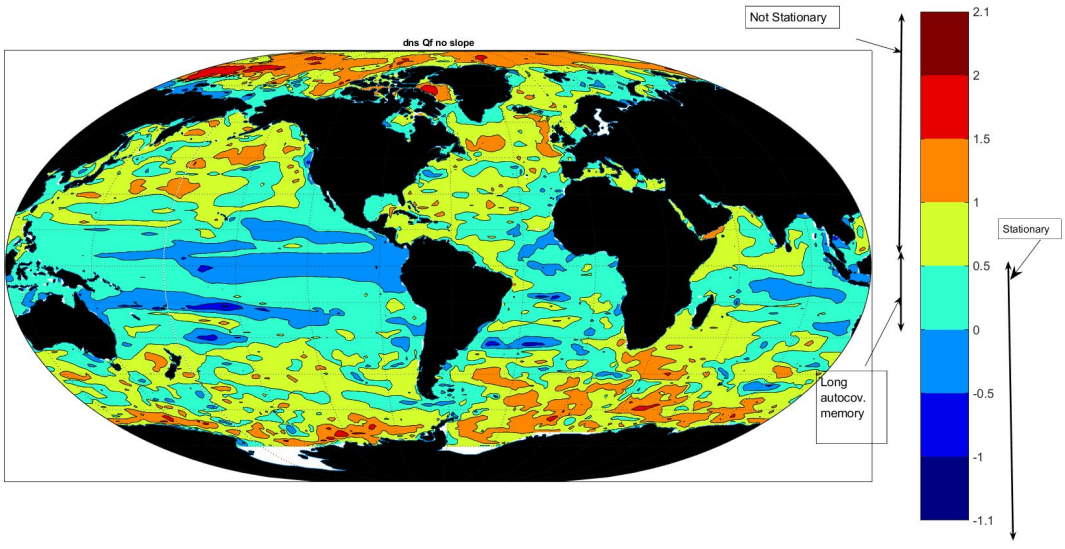

FIG. 21. $\tilde{d}_{NS}$ for the full water column heat content. Now the South Atlantic and South Pacific Oceans have more similar values as long autocovariance memory regions, as well as significant areas of ordinary ARMA processes ($\tilde{d} \leq 0$).

here is consistent with the earlier results of Xu and Fu (2012), Dangendorf et al. (2014) and many others—showing strong global variations in time-integral measures of frequency content.

For some ranges of values $\tilde{d}$, statistical theory suggests that the formal uncertainty (or confidence limits) of a mean or trend can be considerably greater than values computed by conventional means. Here, some estimates appear to be better determined than previously published values. That behavior can be explained as owing to the confinement of the estimates to the period post-1992 of quasi-global data; the use simultaneously of a wide variety of data (e.g., Argo and elephant seal profiles, altimetric measurements, gravity disturbances, moored instrument velocities, etc.); and the information content of the Navier-Stokes equations in their model approximation, but these values are offered only as interim estimates pending improved understanding of the structure of the data and model.

That the ocean contains, even after multi-decadal averaging, a spatially complicated variation in local physics is no surprise. The extent to which those regions have shifted over very long periods is unknown, and in general, the relationship between a modern temporal average of duration T_D and one from a hypothetical much longer duration also remains unknown. What is clear is that

the spatially varying physics (see for example,Hughes and Williams (2010), Xu and Fu, 2012, or Sonnewald et al., 2019) introduces a serious inhomogeneity into calculations of global averages. That difficulty exists, in addition, to questions about adequate observational sampling, particularly in the presence of the complex shape of the sea floor and land-ocean boundaries. An accurate estimate of the uncertainty of global mean sea level or heat or their trends evidently requires a complex weighting of the values at each grid point and including careful consideration of the non-Gaussian distributions. Discussions of global climate change must, apparently, consider major regional differences in the physics and chemistry of ocean-atmospheric interactions (among others). The results strongly support the implication that ocean/atmosphere climate understanding requires both (A) global coverage; (B) strong regional distinctions.

Among the many further applications of the statistical machinery in this paper that have not been pursued, are the ability to do predictions with skill, depending upon the ARIMA structure. For sea level, $\eta(\mathbf{r},t)$, predictions in specific areas are of intense practical interest—albeit the skill will depend upon the particular parameters $\tilde{d},\tilde{p},\tilde{q}$ and is also an application where the multivariable forms of the ARIMA could prove highly useful in particular regions. That the ocean retains a strong regionality in physical properties, likely with arbitrarily extended durations, implies that the physics of climate via air-sea interactions is unlikely in many cases to have dominant global average properties, and must be analyzed dynamical/kinematic region by region.

Values of d or of the Hurst parameter, H, determine the behavior of various statistical estimates that can be applied to state estimate output, most notably means and trends. Results here are best regarded as a set of maps of the behavior of the frequency spectra as the frequency, s, approaches zero. Various regions are those of apparently stationary and non-stationary, of long-autocovariance memory, and of short-memory behavior. Regional prediction has to account for these qualitative changes in statistical structure.

Acknowledgments. I had useful comments on various drafts of this paper by P. Huybers, J.-S. von Storch, S. Griffies, and M. Mudeslee, but consensus is not implied. P. Austin provided useful information on the parallel issues in epidemiology. Assistance with publishing costs was provided by the Cecil and Ida Green Professorial Chair at MIT. Computations reported here were all carried out using MATLAB.

Data availability statement. No original data were generated in this work. The ECCO(v4r4) estimate is publicly available on the NASA website.

APPENDIX

Statistical Framework: ARMA, ARIMA, Wavenumbers

As described in a number of textbooks (e.g.,Priestley, 1982; Brockwell and Davis,1991; Box et al., 2008) the general machinery of ARMA (autoregressive moving average) and ARIMA (autoregressive integrated moving average) processes provides a useful framework for discussion of many linear time series. Consider the ARMA representation and its AR (autoregressive) and moving average (MA) subsets. Let a time series, $\xi(\mathbf{r},t)$, be measured or inferred at discrete time intervals $\Delta t = 1$, at position $\mathbf{r}$ and let B denote a backwards in time operator:

$$B\xi(\mathbf{r},t) = \xi(\mathbf{r},t-1) \tag{A1}$$

Then if $\xi(\mathbf{r},t)$ is a stationary linear process, it can be described accurately in the ARMA(p,q) form of Eq. (4), which when written out is,

$$\xi(\mathbf{r},t) - \phi_1\xi(\mathbf{r},t-1) - \phi_2\xi(\mathbf{r},t-2) - \phi_3\xi(\mathbf{r},t-3) \ldots - \phi_p\xi(\mathbf{r},t-p) = \tag{A2}$$

$$\varepsilon(\mathbf{r},t) - \psi_1\varepsilon(\mathbf{r},t-1) - \psi_2\varepsilon(\mathbf{r},t-2) - \ldots - \psi_q\varepsilon(\mathbf{r},t-q)\,,\ \Delta t = 1 \tag{A3}$$

$\varepsilon(t)$ is commonly a white noise (uncorrelated) random process. The coefficient polynomials are generally expected to be well-behaved (in particular, to be of finite length). As the textbooks explain, for stationary time series the polynomials are "invertible" (stable), so that e.g., one can convert between AR, MA, and ARMA forms, e.g.,

$$\xi(\mathbf{r},t) = \phi(B)^{-1}\psi(B)\,\varepsilon(\mathbf{r},t)\,, \tag{A4}$$

the MA, requiring that in the complex z plane, $\phi(B=z)$ polynomial should have no zeros on the unit circle $|z| = 1$, for $z = \exp(-2\pi i s)$ where s is the angular frequency. If the polynomials are suitably behaved, $\xi(\mathbf{r},t)$ are also then stationary (in the statistical sense). The polynomials can extend to infinite order, but generally diminish so rapidly they can be truncated with little

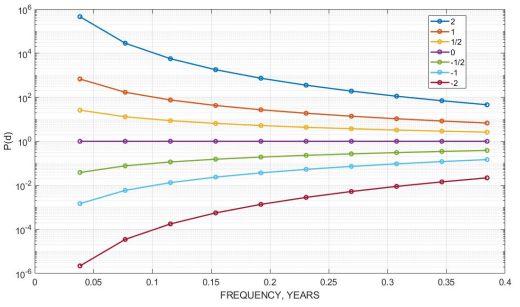

FIG. A1. Semi-log plots of the spectral dependence upon parameter d and used to determine the behavior of the various time series as frequency $s \longrightarrow 0$. These curves are all straight lines on a log-log plot and $\tilde{d}$ is derived from the best-fitting straight line.

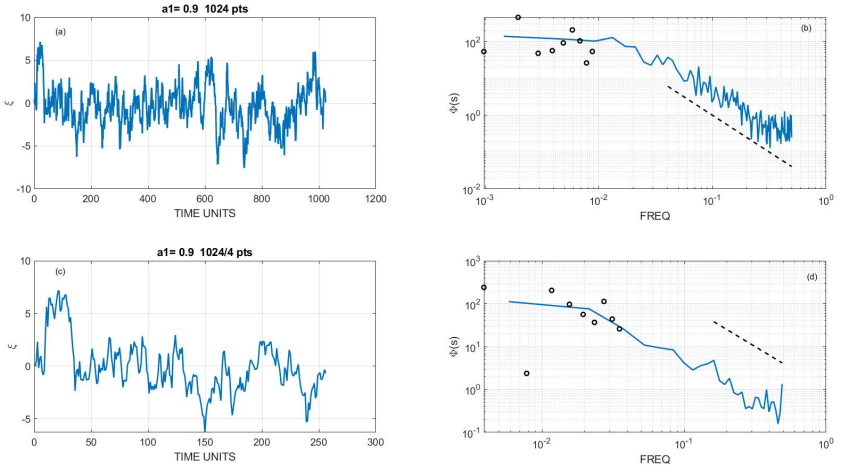

FIG. A2. Time series for $a_1 = 0.9$ and its multitaper spectra using both 1024 and 256 points (panels (a),(c)). (a) might lead one to assert the presence of a trend, but the variability is purely that of a random accumulation of the AR(1). (b), (d) show the periodograms O, as well as the spectra (solid line). Dashed line are s^{-2} reference curves.

loss in accuracy (or prediction skill). Depending upon the particular situation, $\xi(\mathbf{r},t)$ may be thought of as extending backwards in time to $t = -\infty$, or having started at $t = 0$ with known values $\xi(\mathbf{r},0), \xi(\mathbf{r},-1), ...$, sufficient to compute $\xi(\mathbf{r},t), t > 0$. Strict stationarity is then lost for $t > 0$, until such time as memory of the starting values is (possibly) lost.

Let Eq. (5) be the Fourier transform of $\xi(\mathbf{r},t)$, starting at $t = 0$ and extending to N observations (and is a polynomial in z, the z-transform). Then the periodogram is defined in Eq. (6). The

power density, $\Phi(\mathbf{r},s_n)$ is then a smoothed version of $P(\mathbf{r},s_n)$, computed so as to reduce the variance of the elements of $P(s_n)$. The periodogram of the ARMA(p,q) becomes (Eq. (7) for fixed $\mathbf{r}$ Brockwell and Davis (1991, P. 377). For present purposes, the important point is the assumption that $P(\mathbf{r},s_n)$ is a well-behaved, smooth, finite function as $s_n \rightarrow 0$. Generally speaking, frequency domain analyses are more readily physically interpretable than equivalent ones based on autocovariances. d is then estimated from the slope in log frequency of the log periodogram as the period approaches the record length (See Fig. A1). Fig. A2 displays the time series of a simple AR(1), $a_1 = 0.9$ and the behavior of both the periodograms and power density spectra at the lowest frequencies for two different durations. The short duration time series in panel (c) might give the impression of a temporal trend, but it is merely the random fluctuation near the start of the longer series.

The number of terms in the polynomials, p,q determine how far back into the past $\xi(\mathbf{r},t)$ will depend upon its own previous values (determined by the autocorrelation or autocovariance) and/or earlier disturbances $\varepsilon(\mathbf{r},t)$. For stable polynomials, it can be confirmed that the corresponding autocovariance, $\varphi_{\xi\xi}(\mathbf{r},t)$, goes to zero at finite lags. Statistical stationarity requires that at $s = 0$, the periodogram of $\xi(\mathbf{r},t)$, as derived from Eq. (4) or equivalent, is finite.

The literature cited shows that for a *non-stationary* $\xi(\mathbf{r},t)$, a stationary representation can often be obtained by taking temporal differences: for example, sometimes for non-stationary $\xi(\mathbf{r},t)$, $w(\mathbf{r},t) = (1-B)^d \xi(\mathbf{r},t)$ is a process of "stationary increments." See the main text for discussion. Once d, and hence $w(\mathbf{r},t)$, are found, an ARMA is fit to the resulting stationary time series and which becomes an ARIMA(p,d,q) as,

$$\phi(B)\nabla_d \xi(\mathbf{r},t) = \psi(B)\varepsilon(\mathbf{r},t), \tag{A5}$$

or its various rearrangements (that is, the stationary difference series is an ARMA). In much use of this form, d is a small positive integer, and the series in Eq. (9) has only a finite number of terms. But it is also useful to permit it to have an arbitrary, non-integer, value (Granger, 1980, Brockwell and Davis (1991, P. 520+, Beran 1994).

The *inverse* polynomial, for finding ξ from the stationary $\nabla_d \xi(\mathbf{r},t)$ is, for any finite d,

$$\begin{aligned}\nabla_d^{-1} &= (1-B)^{-d} \\ &= 1 - dB + d(d-1)B^2/2! - d(d-1)(d-2)B^3/3! + ... \\ &= \sum_{k=0}^{\infty} \frac{\Gamma(k-d)}{\Gamma(k+1)\Gamma(-d)} B^k .\end{aligned} \tag{A6}$$

and which by using $\phi(B)^{-1}\nabla_d^{-1}$ permits statistical reconstruction of the original time series $\xi(\mathbf{r},t)$ (not done in this paper). For integer $d > 0$, the series in Eq. (A6) extends to infinity—implying that the infinite past of $\xi(\mathbf{r},t)$ is remembered at any time t, unless a given start time value, at $t = 0$ is known, with $\xi(\mathbf{r},t) = 0,\ t < 0$, producing a non-stationary starting transient. The possibility of non-integer d, leading to "fractionally integrated processes," proves useful. For integer $d \geq 1$, Box et al. (2008) provide an extensive discussion of representations dependent upon p, q as well as d—that is including non-stationary processes.

Simple Autoregression.

To have some further context, consider the simplest autoregressive (AR) process of order 1,

$$\xi(t) = a_1 \xi(t - \Delta t) + \varepsilon(t),\ t = 1, 2, ..., \Delta t = 1, \tag{A7}$$

where $\varepsilon(t)$ is zero-mean Gaussian white noise. Numerous textbooks (e.g., Box et al., 2008) discuss the properties of such series at great length, including methods for best-estimating $a_1, \varepsilon(t)$. (If $a_1 = 1$, $\xi(t)$ is a random walk; values greater than 1 change the behavior qualitatively leading to "explosive" time series.) Then taking the discrete Fourier transform,

$$\hat{\xi}(s_n) = a_1 \hat{\xi}(s_n) \exp(-2\pi i s_n) + \hat{\varepsilon}(s_n),\ s_n \leq \frac{1}{2} \tag{A8}$$

or

$$\hat{\xi}(s_n)\left(1 - a_1 e^{-2\pi i s_n}\right) = \hat{\varepsilon}(s_n) \tag{A9}$$

or

$$\left|\hat{\xi}\left(s_n\right)\right|^2 = \frac{\left|\hat{\varepsilon}\left(s_n\right)\right|^2}{\left|1 - a_1 e^{-2\pi i s_n}\right|^2} = \frac{\left|\hat{\varepsilon}\left(s_n\right)\right|^2}{1 + a_1^2 - 2a_1 \cos\left(2\pi s_n\right)} \tag{A10}$$

is the periodogram and s_n the Fourier series frequencies. Taking the expected value on both sides, the power spectrum is,

$$\Phi\left(s_n\right) = \frac{\sigma_\varepsilon^2}{1 + a_1^2 - 2a_1 \cos\left(2\pi s_n\right)}. \tag{A11}$$

Fig. A2 shows realizations of 1024 and 256 points (a), (c) for one choice of $\varepsilon(t)$ and the periodograms and the spectral density for $a_1 = 0.9$, and two durations (again, $\Delta t = 1$), the periodograms (b), (d) and spectra show a steep decline as, roughly s^{-2}, for high frequencies (dashed line), becoming near white noise as $s \to 0$.

As $a_1 - > 1$, it is easily seen from Eq. (A11) that $\Phi\left(s_n\right)$ becomes very large and deducing that the time series is that of an AR(1), rather than an ARIMA with $d = 1$, is an example of the modelling ambiguity that underlies this entire subject. Textbooks emphasize the importance of visual inspection of records and the importance of physical insight, where available, in resolving the corresponding ambiguity.

Wavenumber Statistics

Existence of continental margins and the limitations to a sphere means that the wavenumber spectrum of spatial samples is necessarily non-stationary; but is also not dependent upon any wavelength greater than the longest space scale present in the oceans, probably one of order 10,000km Thus it is *not* a long memory process in either sense in the purely spatial domain and more conventional statistical estimates apply, albeit the underlying process is not stationary. Structures on a sphere require special handling. Goff and Jordan (1988) and others have produced regionally useful wavenumber spectra, and see Radko (2023) for discussion of the physical effects of topography in the spatial domain.

References

Adcroft, A., C. Hill, and J. Marshall, 1997: Representation of topography by shaved cells in a height coordinate ocean model. Mon. Weath. Rev., **125**, 2293-2315.

Anderson, D. L. T., K. Bryan, A. E. Gill, and R. C. Pacanowski, 1979: Transient-response of the North Atlantic - some model studies. J. Geophys. Res. **84**, 4795-4815.

Beran, J., 1994: Statistics for Long Memory Processes. 315 pp.

Beran, J., F. Y., Ghosh S., and R. Kulik, 2013: Long-memory Processes : Probabilistic Properties and Statistical Methods. Springer.

Box, G. E. P., G. M. Jenkins, and G. C. Reinsel, 2008: Time Series Analysis : Forecasting and Control. 4th ed. John Wiley, xxiv, 746 p. pp.

Brockwell, P. J., and R. A. Davis, 1991: Time Series: Theory and Methods 2nd Ed. Springer-Verlag, 577 pp.

Cazenave, A., and L. Moreira, 2022: Contemporary sea-level changes from global to local scales: A review. Proc. Roy. Soc. A, 478, 20220049.

Charette, M. A.,and W. H. F. Smith, 2010: The volume of Earth's ocean. Oceanog., 23, 112-114.

Chatfield, C., 2004: The Analysis of Time Series. An Introduction, Sixth Ed. Chapman and Hall/CRC.

Fukumori, I., O. Wang, I. Fenty, G. Forget, P. Heimbach, and R. M. Ponte, 2019: ECCO Version 4 Release 4,https://ecco.jpl.nasa.gov/drive/files/Version4/Release4/doc/v4r4_synopsis.pdf.

Gebbie, G., and P. Huybers, 2019: The Little Ice Age and 20th-century deep Pacific cooling. Science, 363, 70-+.

GEBCO Compilation Group, 2024: GEBCO 2024 Grid doi:10.5285/1c44ce99-0a0d-5f4f-e063-7086abc0ea0f

Gil-Alana, L. A., 2012: Long memory, seasonality and time trends in the average monthly temperatures in Alaska. Theor. Appl. Climatol., 108, 385-396.

Gil-Alana, L. A., 2012: Long memory, seasonality and time trends in the average monthly temperatures in Alaska. Theoretical and Applied Climatology, 108, 385-396.

Gil-Alana,L. A., R. Gupta, L. Sauci, and N. Carmona-Gonz?lez, 2022: Temperature and precipitation in the US states: long memory, persistence, and time trend. Theor. Appl. Climatol., 150, 1731-1744.

Goff, J. A., and T. H. Jordan, 1988: Stochastic modeling of seafloor morphology-inversion of sea beam data for 2nd-order statistics. Journal of Geophysical Research-Solid Earth and Planets, 93, 13589-13608.

Goh, C., and R. Law, 2002:Modeling and forecasting tourism demand for arrivals with stochastic nonstationary seasonality and intervention. Tourism Managem. 23, 499-510.

Hurvich, C. M: Ray, B. K., 1995: Estimation of the memory parameter for nonstationary or noninvertible fractionally integrated processes. J. Time Series Anal., 16, 17-41.

Heimbach, P., C.Wunsch, R. M. Ponte, G. Forget, C. Hill, and J. Utke, 2011: Timescales and regions of the sensitivity of Atlantic meridional volume and heat transport magnitudes: Toward observing system design. Deep-Sea Res.-II, 58, 1858-1879.

Johnson, G. C., and S. G. Purkey, 2024: Refined estimates of global ocean deep and abyssal decadal warming trends. Geophys. Res. Lett., 51, c2024GL.111229, https://doi.org.10.1029/2024GL.111229.

Kalmikov,A., and P. Heimbach, 2014: A Hessian-based method for uncertainty quantification in global ocean state estimation. SIAM J. Sci. Comput., 36, S267-S295.

Liang, X., C. Wunsch, P. Heimbach, and G. Forget, 2015: Vertical redistribution of oceanic heat content. J. Clim., 28, 3821-3833.

Liu, C., X. Liang, R. M. Ponte, and D. P. Chambers, 2024: "Salty Drift" of Argo floats affects the gridded ocean salinity products. J. Geophys. Res., Oceans 129, e2023JC020871.

Mudelsee,M., 2014: Climate Time Series Analysis: Classical Statistical and Bootstrap Methods. Second edition. ed. Springer.

Overland, J. E., D. B.Percival, and H. O. Mofjeld, 2006: Regime shifts and red noise in the North Pacific. Deep-Sea Res. I,, 53, 582-588.

Percival, D. B., and D. A. Rothrock, 2005: "Eyeballing" trends in climate time series: A cautionary note. J. Clim., 18, 886-891.

Percival, D. B., J. E. Overland, and H. O. Mofjeld, 2001: Interpretation of North Pacific variability as a short- and long-memory process. J. Clim., 14, 4545-4559.

Ponte

Priestley, M. B., 1981: Spectral Analysis and Time Series. Academic Press, 2 v. (xvii, 45, 890 pp.)

827 Pugh, D., and P. L. Woodworth, 2014: Sea-Level Science : Understanding Tides, Surges,
828 Tsunamis and Mean Sea-Level Changes. Second edi. Cambridge Un. Press, xii, 395 pages pp.
829
830 Radko, T., 2023: A generalized theory of flow forcing by rough topography. J. Fluid Mechs.,
831 961, A24.
832
833 Sonnewald, M., C. Wunsch, and P. Heimbach, 2019: Unsupervised learning reveals geography
834 of global ocean dynamical regions. Earth Space Sci, 6, 784-794.
835
836 Thorpe, S. A., 2005: The Turbulent Ocean. Cambridge Un. Press, 439 p..
837
838 von Schuckmann, K., and Coauthors, 2023: Heat stored in the Earth system 1960–2020: where
839 does the energy go? Earth Syst. Sci. Data, 15, 1675-1709
840
841 Wunsch, C., 1999: The interpretation of short climate records, with comments on the North
842 Atlantic and Southern Oscillations. Bull. Am Met. Soc., 80, 245-255.
843
844 Wunsch, C., 2006: Discrete Inverse and State Estimation Problems: With Geophysical Fluid
845 Applications. Cambridge Un. Press, xi, 371 pp.
846
847 Wunsch, C., 2015: Modern Observational Physcial Oceanography. Princeton Un. Press, 493
848 pp.
849
850 Wunsch, C., 2018: Towards determining uncertainties in global oceanic mean values of heat,
851 salt, and surface elevation heat, salt, and surface elevation. Tellus 70, 1-14.
852
853 Wunsch, C., 2024: A time-average ocean: Thermal wind and flow spirals. Prog. oceanog., 221,
854 https://doi.org/10.1016/j.pocean.2024.103206
855

Wunsch, C., 2024: Patterns of kinetic energy conversion in a time-average upper ocean. Submitted for publication.

Wunsch, C., and P. Heimbach, 2008: How long to ocean tracer and proxy equilibrium? Quat. Sci. Rev., 27., doi:10.1016/j.quascirev.2008.1001.1006, 1639-1653.

Wunsch, C., 2014: Bidecadal thermal changes in the abyssal ocean and the observational challenge. J. Phys. Oc., 44, 2013-2030.

Xu, Y. S., and L. L. Fu, 2012:The effects of altimeter instrument noise on the estimation of the wavenumber spectrum of sea surface height. J. Phys. Co., 42, 2229-2233.